

STUDIES OF IMBALANCE DIFFERENCE THEORY IN MODELING
CONVERSION BETWEEN DIFFERENTIAL MODE AND COMMON MODE
SIGNALS

A Dissertation
Presented to
the Graduate School of
Clemson University

In Partial Fulfillment
of the Requirements for the Degree
Doctor of Philosophy
Automotive Engineering

by
Li Niu
December 2014

Accepted by:
Todd Hubing, Committee Chair
Robert Prucka
Simona Onori
Pierluigi Pisu

UMI Number: 3680740

All rights reserved

INFORMATION TO ALL USERS

The quality of this reproduction is dependent upon the quality of the copy submitted.

In the unlikely event that the author did not send a complete manuscript and there are missing pages, these will be noted. Also, if material had to be removed, a note will indicate the deletion.



UMI 3680740

Published by ProQuest LLC (2015). Copyright in the Dissertation held by the Author.

Microform Edition © ProQuest LLC.

All rights reserved. This work is protected against unauthorized copying under Title 17, United States Code



ProQuest LLC.
789 East Eisenhower Parkway
P.O. Box 1346
Ann Arbor, MI 48106 - 1346

ABSTRACT

This dissertation describes three related studies regarding the imbalance difference theory in modeling the conversion between differential mode and common mode/antenna mode signals. The topics covered are: rigorous derivation of imbalance difference theory for modeling radiated emission problems, modeling the conversion between differential mode and common mode propagation in transmission lines, and modeling the loading impedance on differential mode signals due to radiated emissions.

The imbalance difference theory describes a method for calculating the coupling between differential mode signals and common mode signals due to changes in electrical balance on a transmission line. It provides both physical insight and a simple technique for modeling the conversions between the two modes.

The first chapter presents a rigorous derivation of imbalance difference theory for modeling radiated emission problems. Although the theory has been successfully used to model a wide variety of important EMC problems over the past, it has not been rigorously derived. The derivation carefully defines the important quantities and demonstrates that imbalance difference calculations are exact provided that the differential-mode propagation is TEM and the current division factor, h , represents the actual ratio of currents on the two transmission line conductors excited by a common-mode source. This chapter also discusses the acquisition of the current division factor from 2D calculations of the cross-section of the transmission line.

The second chapter provides a rigorous development of the imbalance difference theory for three-conductor transmission lines where both the differential mode and

common mode exhibit TEM propagation. It also derives expressions for the mode conversion impedances, which account for the energy converted from one mode to the other. They are essential for modeling the conversion between the two modes when they are strongly coupled.

The third chapter introduces conversion impedance to the existing imbalance difference theory model for modeling radiated emission problems, so that when the coupling between differential mode and antenna mode are strong, the imbalance difference theory can more accurately estimate the antenna mode current.

All three papers are about confirming, enriching and expanding the imbalance difference theory. The first chapter focuses on the rigorous derivation of theory for its most common application, radiated emission problems. The second chapter expands the theory to multi-conductor transmission line structure when the two modes are strongly coupled. The last chapter introduces conversion impedance to the theory in modeling radiated emission problems and improves the accuracy of the model at resonant frequencies.

ACKNOWLEDGMENTS

First, I would like to thank my parents, who received very little education but have been working extremely hard throughout their lives. In the 28 years of my life, they not only gave me unconditioned love, caring, encouragement and inspiration, more importantly, they showed me with their own conduct how to be a hard-working and kind person. They are the reason for who I am today and they are the single most precious gift I ever had from god.

Second, I would like to thank my advisor, Dr. Todd Hubing, who has been teaching me, supporting me and mentoring me for more than 5 years now. His passion for EMC, expertise and wisdom have kept inspiring and motivating me. He is the reason I am determined to pursue EMC as my life-long career. His kindness to people, diligence to work, modesty to colleagues and always-positive attitude to life have always been something I watched and learned over the years. He was, is and will always be my idol, it was so lucky to be a student of his and I wish someday I can be a person just like him.

Third, I want to thank all the professors that I met at Clemson, including my committee members: Dr. Robert Prucka, Dr. Simona Onori, Dr. Pierluigi Pisu, for their support and help; cours insctructors, Dr. Ardalan Vahidi, Dr. Thomas Kurfess, Dr. Paul Vehovens, Dr. Beshah Ayalew, Dr. Steve Hung, Dr. Imtiaz Haque, Dr. John Ziegert, Dr. Pingshan Wang, Dr. Xiaobang Xu, Dr. Anthony Martin and Dr. Wilson Pearson. I learned so much from them.

Last, I want to thank all the staffs at Clemson University that have helped me and all the friends I met, together with whom, I feel Clemson is like home.

TABLE OF CONTENTS

	Page
TITLE PAGE	i
ABSTRACT	ii
ACKNOWLEDGMENTS	iv
LIST OF TABLES	vii
LIST OF FIGURES	viii
CHAPTER	
I. CHAPTER ONE	
RIGOROUS DERIVATION OF IMBALANCE DIFFERENCE THEORY FOR MODELING RADIATED EMISSION PROBLEMS	1
1.1 Introduction	1
1.2 Definitions of differential mode and antenna mode signals on the transmission lines	3
1.3 Conversion between DM signals and AM signals on TLs	7
1.4 Calculation of current division factor	13
1.5 Example structures	15
1.6 Conclusion	19
II. CHAPTER TWO	
MODELING THE CONVERSION BETWEEN DIFFERENTIAL MODE AND COMMON MODE PROPAGATION IN TRANSMISSION LINES	22
2.1 Introduction	22
2.2 Definitions of differential mode and common mode signals	25
2.3 Conversion between DM signals and CM	29
2.4 Models of the differential mode to common mode conversion	31
2.5 Demonstration example	35
2.6 Conclusion	40
III. CHAPTER THREE	
MODELING THE LOADING IMPEDANCE ON DIFFERENTIAL	

Table of Contents (Continued)	Page
MODE SIGNALS DUE TO RADIATED EMISSIONS.....	49
3.1 Introduction.....	49
3.2 Imbalance difference theory	51
3.3 Experimental validation.....	54
3.4 Conclusion	61

LIST OF TABLES

Table		Page
2.1	Capacitances calculated by ATLC2	35
2.2	Comparison of calculation result with different method	40
3.1	Parameters of measurement setup.....	55

LIST OF FIGURES

Figure	Page
1.1 Two two-conductor TLs with different cross sections connected end-to-end.	4
1.2 The antenna-mode voltage at the interface between the TLs.	4
1.3 Antenna mode of TLs with divided AM current	5
1.4 Differential-mode voltage at the interface of two two-conductor TLs	6
1.5 Equivalent AM circuit.....	7
1.6 Decomposition of AM circuit (1/2)	7
1.7 Decomposition of AM circuit (2/2)	8
1.8 Decomposition of AM circuit (1/2)	9
1.9 Decomposition of AM circuit (2/2)	9
1.10 Equivalent AM circuit.....	10
1.11 Equivalent AM circuit (1/2).....	10
1.12 Equivalent AM circuit (2/2).....	10
1.13 An equivalent circuit of the original circuit in Fig. 1.1	11
1.14 An equivalent circuit of the original circuit in Fig. 1.1	11
1.15 Decomposition of the original circuit (1/2)	11
1.16 Decomposition of the original circuit (2/2)	12
1.17 Illustration of electric field distribution resulted from a quasi-static source driving a two-conductor transmission line relative to another wire	14
1.18 Illustration of electric field distribution resulted from a quasi-static source driving a two-conductor transmission line relative to another angled wire.	14
1.19 Example Structure 1.....	16

List of Figures (Continued)

Figure	Page
1.20 Example structure 2	16
1.21 Example structure 3	17
1.22 Current division factor calculation result over 30MHz to 200MHz	18
2.1 A two-conductor TL above a reference plane with matching termination ..	26
2.2 Two-conductor TL with a discontinuity of electrical balance above a reference.....	29
2.3 Decomposition of the original circuit into DM and CM propagation	31
2.4 Equivalent model for DM-to-CM conversion.....	31
2.5 Equivalent model for CM-to-DM conversion.....	33
2.6 Example structure in 3D views	35
2.7 The cross-section of the two-conductor transmission line and the reference conductor.....	35
2.8 Per-unit-length capacitances between conductors	36
2.9 HFSS calculation result.....	39
2.10 Lumped LC model for a cross section of TL	45
2.11 Lumped Impedance network of TL	46
3.1 Two-conductor transmission lines with changed corss-section.....	51
3.2 Antenna mode of TLs with divided AM current	51
3.3 DM circuit with the extra virtual DM current.....	53
3.4 DM circuit with the conversion impedance	53
3.5 Validation structure and measurement set up	54

List of Figures (Continued)

Figure
3.6	Validation structure and measurement set up 54
3.7	Equivalent circuit for measurement set up..... 55
3.8	Comparison of DM voltage at the T-connection 58
3.9	Comparison of AM current at the bottom of the antenna 59
3.10	Input impedance of the antenna seen by the AM voltage source 60

CHAPTER ONE

RIGOROUS DERIVATION OF IMBALANCE DIFFERENCE THEORY FOR MODELING RADIATED EMISSION PROBLEMS

Abstract

According to the imbalance difference theory, the conversion between differential mode signals and common mode signals is due to changes in electrical balance. The theory provides both physical insight and a powerful technique for modeling the conversion from differential-mode signals to common-mode noise, especially for radiated emission problems. Although the theory has been successfully used to model a wide variety of important EMC problems over the past 14 years, it has not been rigorously derived. This paper provides a strict derivation of the theory and carefully defines the important quantities. The derivation demonstrates that imbalance difference calculations are exact provided that the differential-mode propagation is TEM and the current division factor, h , represents the actual ratio of currents on the two transmission line conductors excited by a common-mode source. The paper also discusses the acquisition of the current division factor from 2D calculations of the cross-section of the transmission line.

1.1 Introduction

Unintended radiated emission is one of the most challenging EMC problems. It is often caused by the unintended common-mode (CM) currents induced on long wires or metal structures [1][2]. The generation of CM currents from the known differential-mode (DM) signals has been studied extensively over the last two decades. In [3], for typical

printed circuit board (PCB) structures with attached cables, two fundamental common-mode source mechanisms were identified as the *current-driven* mechanism and *voltage-driven* mechanism. Current-driven common-mode currents are caused by the signal currents flowing through the partial inductance of the current return path resulting in an effective voltage drop between different portions of the board. Voltage-driven common-mode currents are caused by the electric-field coupling between the signal trace and the attached wires. Although these coupling mechanisms were intuitive, their application required the user to make approximating assumptions, so the results of the calculations were not precise.

More recently, another approach to the problem of modeling differential-mode to common-mode conversion was introduced [3][4]. This approach is commonly referred to as the Imbalance Difference Theory (IDT). IDT defines the concept of electric balance in a transmission line (TL) and an imbalance factor (also known as current division factor) that precisely quantifies this balance. IDT demonstrates that changes in the electrical balance on TLs results in the conversion from DM signals to CM signals. The amplitude of the induced CM voltage can be accurately expressed as the product of the DM voltage and the change in the imbalance factor at any given point along a transmission line. The IDT provides great insight into the DM-to-CM conversion mechanism and provides an easy way of modeling this conversion in many practical situations. It has been applied to the modeling of many radiated emission problems that would be otherwise difficult to analyze [4]–[17] and has proven to be a very powerful and accurate technique.

Despite its successful application to a wide variety of important EMC problems, IDT has not been widely utilized. Although researchers have shown it to be accurate and reliable, the original papers deriving IDT made simplifying assumptions that seemed to limit the application of the method to structures of little overall interest. The most significant assumption in the original derivation was that both the DM and CM modes exhibited TEM propagation. This appeared to prohibit the application of the theory to radiated emission problems, despite the fact that it seemed to work well for radiated emission modeling.

This paper rigorously derives the IDT for radiated emission problems where no TEM assumption is made for the CM current propagation. To avoid confusion, in this paper we will use the term *antenna mode* (AM), instead of common mode (CM) to describe currents that propagate in one direction on both transmission line conductors without returning on a nearby ground (i.e. the non-TEM case).

1.2 Definitions of Differential Mode and Antenna Mode Signals on the Transmission Lines

Fig. 1.1 shows a pair of two-conductor TLs connected together. The variation in the thicknesses of the bars is to indicate that the left-side TL and the right-side TL may be of different cross sections. The current on each conductor, $I_1(z)$, and $I_2(z)$, are generally functions of position. At the interface where the two TLs connect, these currents are continuous. We label them I_1 and I_2 as shown in Fig. 1.1. Throughout this derivation, quantities that are functions of position along the transmission line will be written as

functions of z . The value of those quantities at the interface will employ the same variables without being expressed as functions of position.

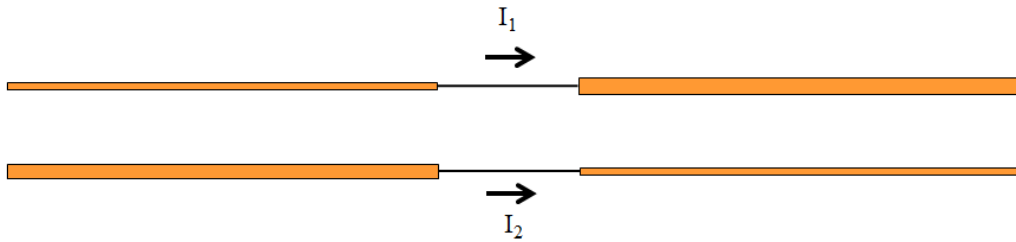


Fig. 1.1. Two two-conductor TLs with different cross sections connected end-to-end.

1.2.1 Definition of Antenna Mode Signals

The antenna-mode current, I_{AM} is defined as the total current that flows on both conductors,

$$I_{AM}(z) = I_1(z) + I_2(z). \quad (1)$$

The antenna-mode impedance at the interface, Z_{AM} , is defined as the input impedance of the antenna that is formed by the conductors in Fig. 1.1 and when it is driven by a source as indicated in Fig.1.2.

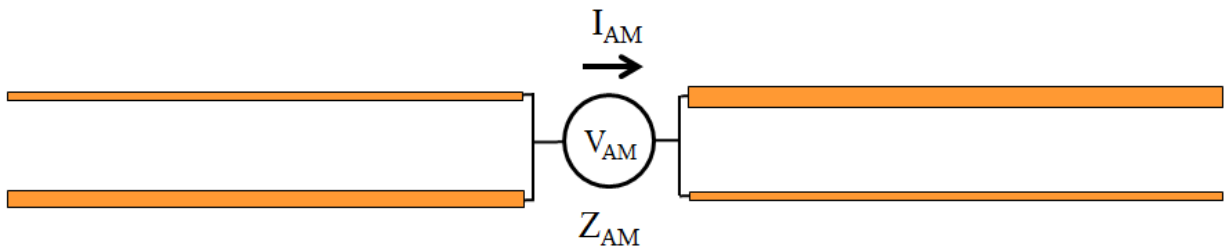


Fig.1.2. The antenna-mode voltage at the interface between the TLs.

The AM voltage, V_{AM} , is defined as the product of the AM current and the AM impedance at the interface,

$$V_{AM} = I_{AM} \cdot Z_{AM} \quad (2)$$

1.2.2 Definition of Current Division Factor

The AM current is carried by both conductors of the TLs. We define the current division factor, h , as the portion of the AM current that flows on one conductor divided by the total AM current flows on both conductors.

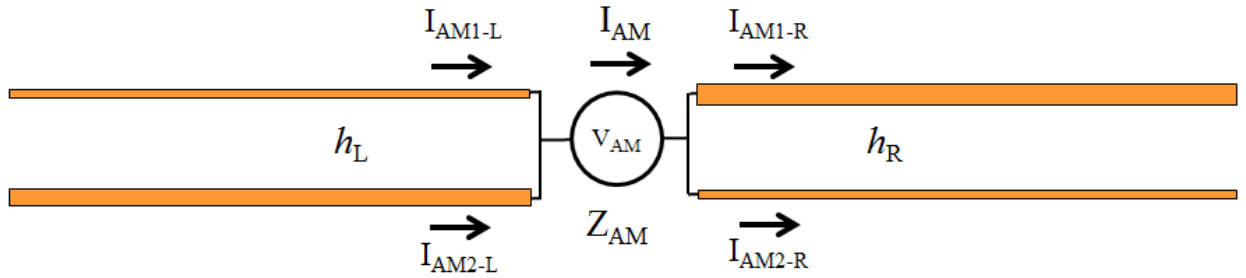


Fig.1.3. Antenna mode of TLs with divided AM current.

In Fig.1.3, I_{AM-1L} , I_{AM-2L} , I_{AM-1R} and I_{AM-2R} denote the current on each conductor of the TLs at the points just to the left and right of the interface, respectively. Due to the continuity of the currents I_1 and I_2 , they satisfy the following relationship:

$$I_{AM} = I_{AM1-L} + I_{AM2-L} = I_{AM1-R} + I_{AM2-R} \quad (3)$$

At the interface, we denote the current division factors for the left-side and right-side of the TL as h_L and h_R . They are defined as,

$$h_L = I_{AM1-L} / I_{AM} \quad (4)$$

$$h_R = I_{AM1-R} / I_{AM} \quad (5)$$

Combining (3), (4) and (5), the AM currents on each conductor can be expressed as:

$$I_{AM1-L} = I_{AM} \cdot h_L \quad (6)$$

$$I_{AM2-L} = I_{AM} \cdot (1-h_L) \quad (7)$$

$$I_{AM1-R} = I_{AM} \cdot h_R \quad (8)$$

$$I_{AM2-R} = I_{AM} \cdot (1-h_R) \quad (9)$$

1.2.3 Definition of Differential Mode Signals

The DM signals on the TLs are TEM, so we can define the DM voltage, $V_{DM}(z)$, as the voltage difference between the two conductors. V_{DM} specifically represents the DM voltage at the interface, as shown in Fig.1.4.

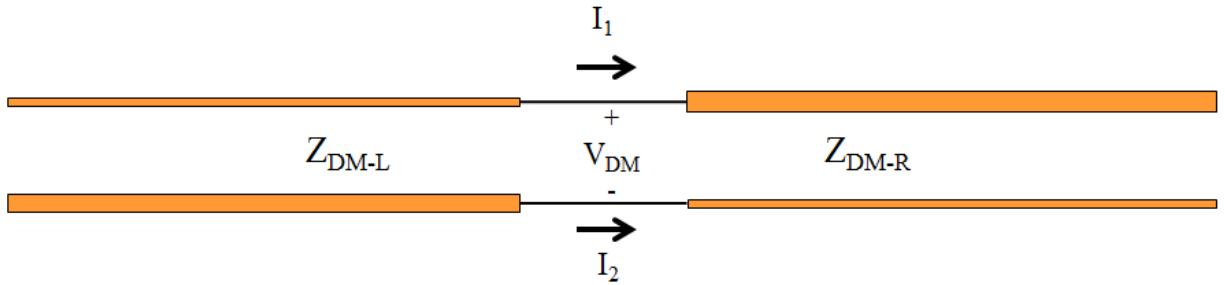


Fig.1.4. Differential-mode voltage at the interface of two two-conductor TLs.

The DM impedance, Z_{DM} , is defined as the characteristic impedance of the TLs. They are denoted as Z_{DM-L} and Z_{DM-R} for the left-side and right-side of the TLs.

The AM current was defined in (1). We want the differential mode and the antenna mode to be orthogonal, so we define the DM current to be any current remaining when the AM current is subtracted from the total current. This means, that the DM components of current should have the same amplitude and opposite direction on each conductor. The DM components of the current on each side of the interface can be expressed as,

$$I_{DM-L} = I_1 - I_{AM1-L} = -(I_2 - I_{AM2-L}) = (1 - h_L) \cdot I_1 - h_L \cdot I_2, \quad (10)$$

$$I_{DM-R} = I_1 - I_{AM1-R} = -(I_2 - I_{AM2-R}) = (1 - h_R) \cdot I_1 - h_R \cdot I_2. \quad (11)$$

1.3 Conversion between DM signals and AM signals on TLs

The AM circuit in Fig.1.3 can be represented equivalently as shown in Fig.1.5. In this figure, the voltages between the 4 conductors at the interface are identical to their values in Fig.1.3.

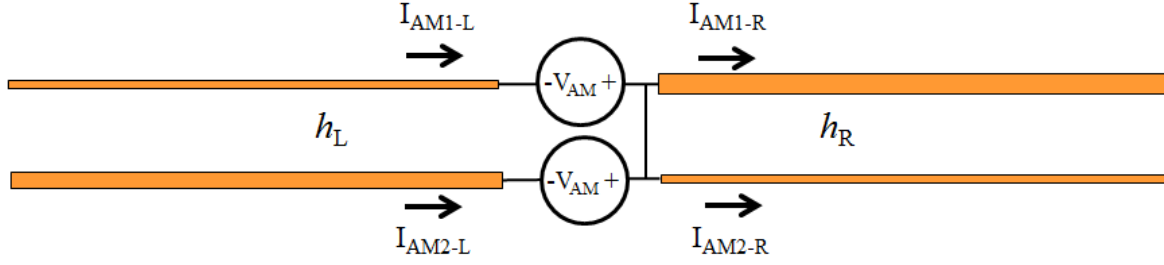


Fig.1.5. Equivalent AM circuit.

Applying superposition, the AM circuit of Fig.1.5 can be decomposed into the two circuits in Fig.1.6 and Fig.1.7.

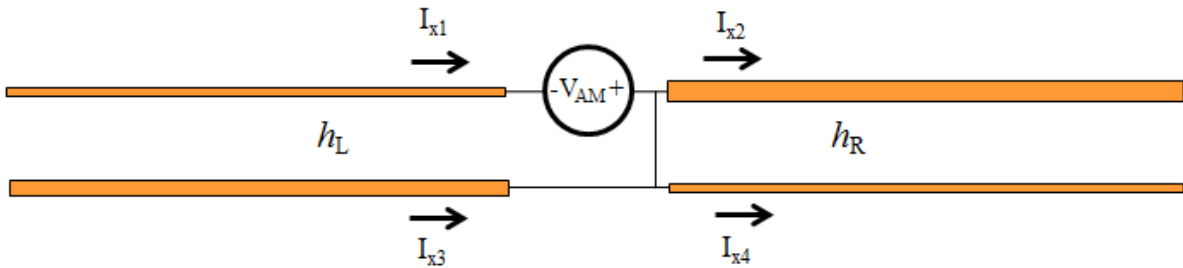


Fig.1.6. Decomposition of AM circuit (1/2).

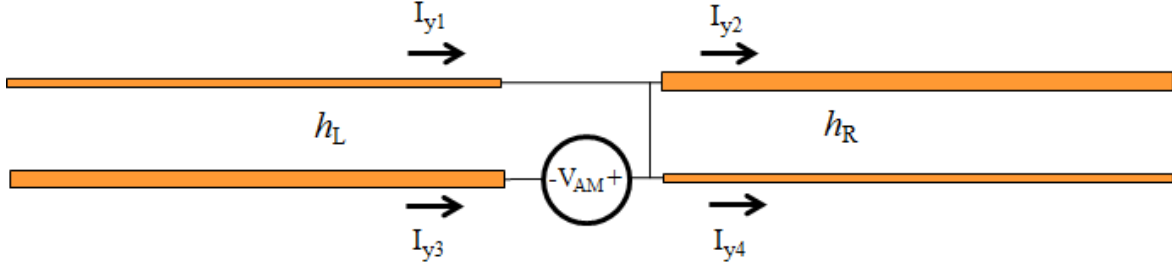


Fig.1.7. Decomposition of AM circuit (2/2).

The current on each conductor in Fig.1.5 can be expressed as the sum of the corresponding current on the same conductor in Fig.1.6 and Fig.1.7 (denoted as “ I_x ”s and “ I_y ”s):

$$I_{AM1-L} = I_{x1} + I_{y1} , \quad (12)$$

$$I_{AM1-R} = I_{x2} + I_{y2} , \quad (13)$$

$$I_{AM2-L} = I_{x3} + I_{y3} , \quad (14)$$

$$I_{AM2-R} = I_{x4} + I_{y4} . \quad (15)$$

The continuity of the current ensures that,

$$I_{x1} + I_{x3} = I_{x2} + I_{x4} \quad (16)$$

$$I_{y1} + I_{y3} = I_{y2} + I_{y4} . \quad (17)$$

In Fig.1.6 and Fig.1.7, the ideal voltage source V_{AM} drives three conductors relative to the fourth one. The configurations in Fig.1.6 and Fig.1.7 can be redrawn equivalently as shown in Fig.1.8 and Fig.1.9, respectively.

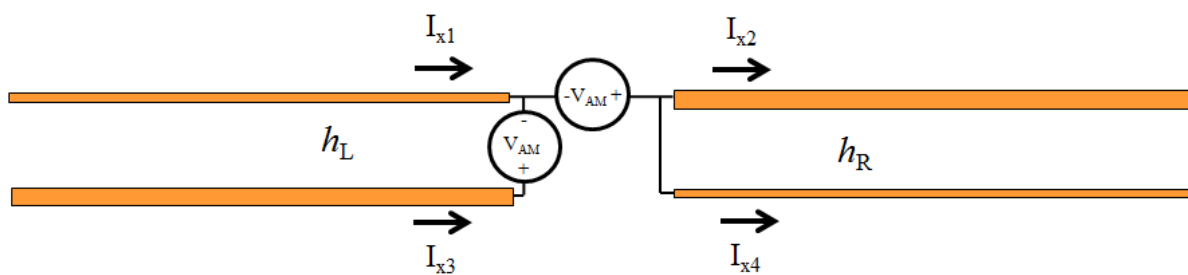


Fig.1.8. Decomposition of AM circuit (1/2).

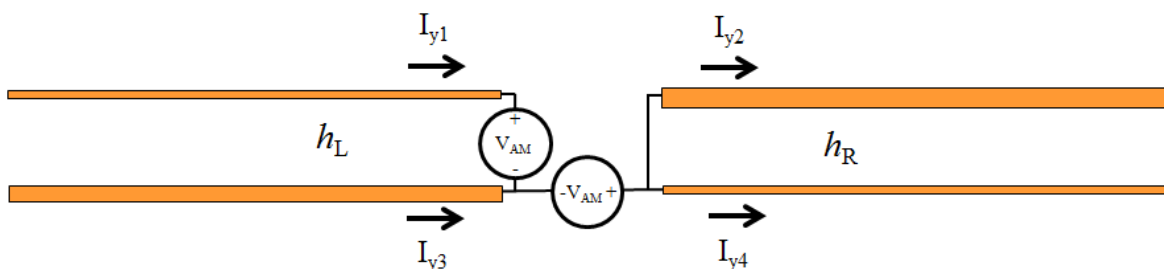


Fig.1.9. Decomposition of AM circuit (2/2).

Examination of these circuits reveals that the current on lower left conductor, I_{x3} in Fig.1.8, and the current on upper left conductor, I_{y1} in Fig.1.9, are due to the same source voltage, V_{AM} , driving the same load impedance, the DM impedance of the left-side TL. As a result these currents are equal,

$$I_{AM1-L} = I_{x1} + I_{x3} = I_{x2} + I_{x4} . \quad (18)$$

It is interesting to note that the total AM current on the circuit in Fig.1.8 is equal to the portion of the AM current that flows on the upper conductor on the left-side TL in Fig.1.3. Similarly, the total AM current in the circuit of Fig.1.9 is equal to the portion of AM current that flows on the lower conductor of the left-side TL in Fig.1.3.

Using the same approach, we can decompose the original AM circuit of Fig.1.3 into two circuits that the AM current of which equals to those on the right-side TL of Fig.1.3. The equivalent circuit and the decomposed circuits are shown in Figs. 10-12.

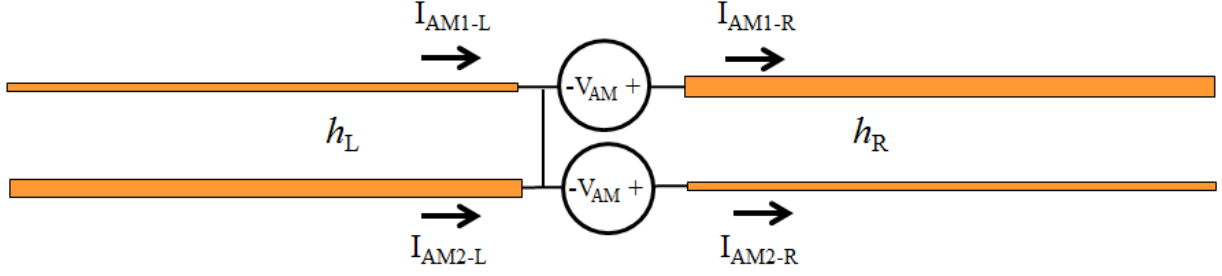


Fig.1.10. Equivalent AM circuit.

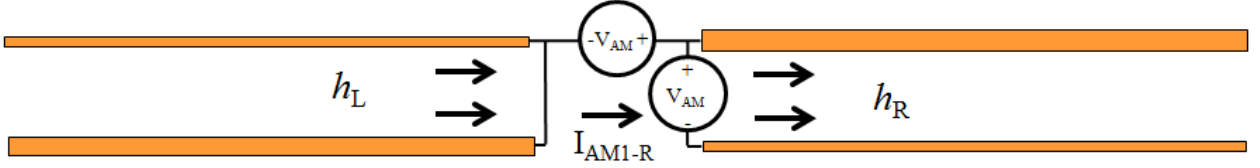


Fig.1.11. Decomposition of AM circuit (1/2).

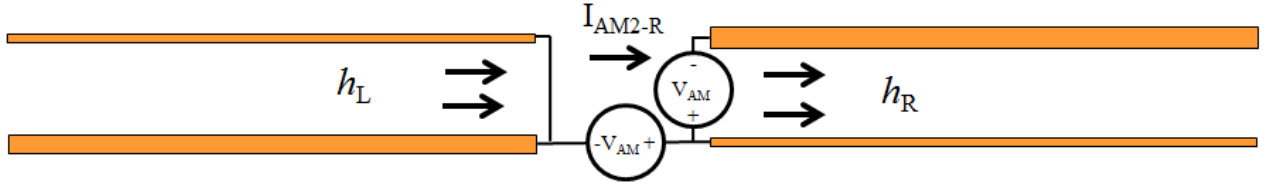


Fig.1.12. Decomposition of AM circuit (2/2).

We can define partial AM impedances as follows,

$$\begin{aligned}
 Z_{AM1L} &\equiv Z_{AM} / h_L, \\
 Z_{AM2L} &\equiv Z_{AM} / (1 - h_L), \\
 Z_{AM1R} &\equiv Z_{AM} / h_R, \\
 Z_{AM2R} &\equiv Z_{AM} / (1 - h_R).
 \end{aligned}
 \tag{19}$$

Partial AM impedances are the impedances seen by the voltage sources in Fig.1.8, Fig.1.9, Fig.1.11 and Fig.1.12. The AM currents associated with these circuits are:

$$\begin{aligned}
 I_{AM1-L} &= V_{AM} / Z_{AM1-L}, \\
 I_{AM2-L} &= V_{AM} / Z_{AM2-L}, \\
 I_{AM1-R} &= V_{AM} / Z_{AM1-R}, \\
 I_{AM2-R} &= V_{AM} / Z_{AM2-R}.
 \end{aligned}
 \tag{20}$$

Referring back to the original circuit in Fig. 1.1, the DM voltage at the interface is V_{DM} . Placing two ideal voltage sources with amplitude of V_{DM} in parallel at the interface, as indicated in Fig.1.13, does not change the currents.

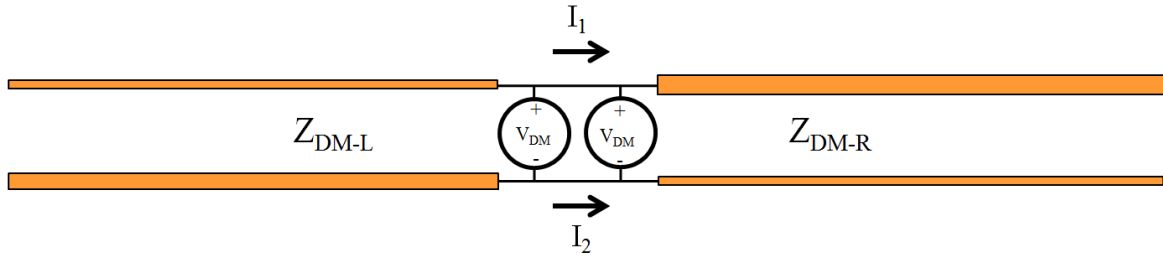


Fig.1.13. An equivalent circuit of the original circuit in Fig. 1.1.

Placing two additional ideal voltage sources in series with the same amplitude, V_{DM} , and opposite sign, as shown in Fig.1.14, does not change the currents either.

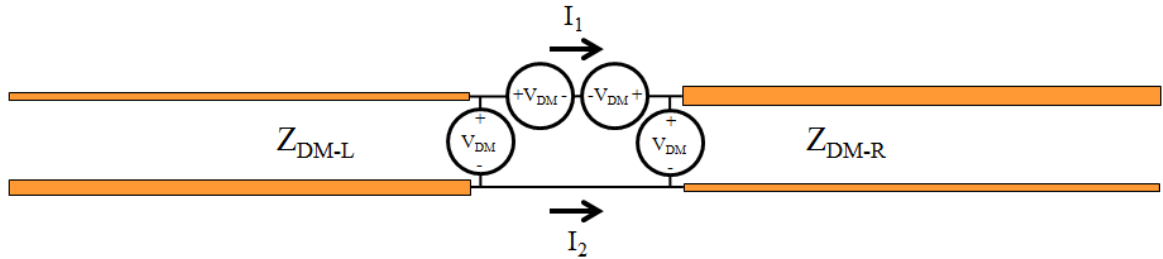


Fig.1.14. An equivalent circuit of the original circuit in Fig. 1.1.

Using superposition, the circuit in Fig.1.14 can be decomposed into the two circuits as shown in Fig.1.15 and Fig.1.16.

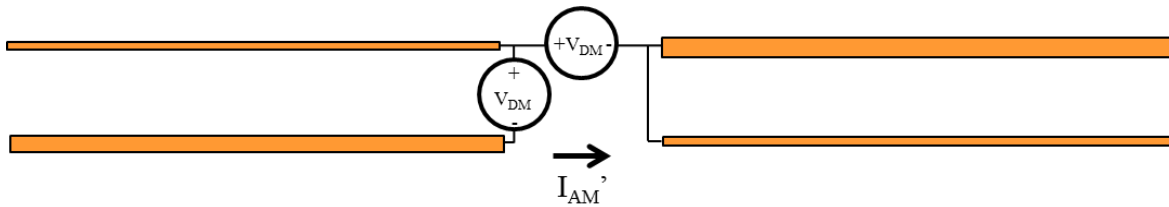


Fig.1.15. Decomposition of the original circuit (1/2).

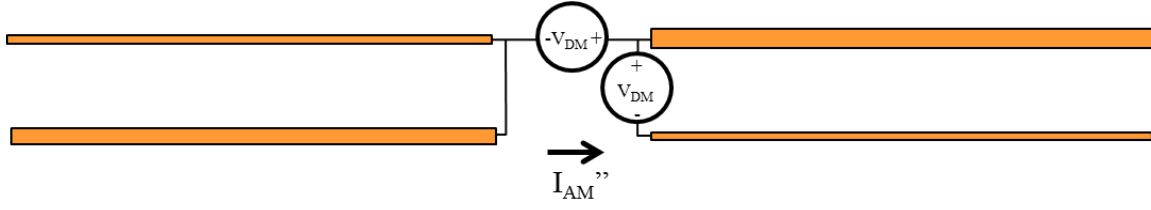


Fig.1.16. Decomposition of the original circuit (2/2).

Other than the amplitude of the voltage sources, Fig.1.15 and Fig.1.16 are identical to the circuits in Fig.1.8 and Fig.1.11. As a result the AM currents, I_{AM}' and I_{AM}'' , generated in Fig.1.15 and Fig.1.16 can be calculated as,

$$\begin{aligned} I_{AM}' &= -V_{DM} / Z_{AM1-L} = -(V_{DM} / Z_{AM}) \cdot h_L, \\ I_{AM}'' &= V_{DM} / Z_{AM1-R} = (V_{DM} / Z_{AM}) \cdot h_R. \end{aligned} \quad (21)$$

The total AM current generated in the original circuit in Fig. 1.1 will be the sum of the AM currents in Fig.1.15 and Fig.1.16:

$$I_{AM} = I_{AM}' + I_{AM}'' = (V_{DM} / Z_{AM}) \cdot (h_R - h_L) . \quad (22)$$

Combining (22) and (2), we can get,

$$V_{AM} = V_{DM} \cdot (h_R - h_L) . \quad (23)$$

Equation (23) is the core equation of the IDT that has been used to model the DM-to-AM conversion in a wide variety of structures. Here, it is shown to be an exact relationship as long as the DM propagation is TEM and the imbalance factors are defined based on the antenna-mode current division as indicated in (4) and (5).

1.4 Calculation of Current Division Factor

1.4.1 Discussion of Previous Calculation Method

In published applications of IDT for radiated emission modeling [4]–[17], the imbalance factors are calculated using one of the following equations [4]:

$$h = \frac{C_{11}}{C_{11} + C_{22}} \quad (23)$$
$$h = \frac{L_{22} - L_{12}}{L_{11} + L_{22} - 2L_{12}}$$

The definitions of imbalance factor in (23) are not strictly equivalent to the current division factors in (4) and (5). In [4], these equations are derived assuming that the AM signals satisfy the telegrapher's equations (i.e. exhibit TEM propagation). In this case, C_{11} , C_{22} , L_{11} , L_{22} and L_{12} are the per-unit-length parameters of a transmission line with a well-defined and nearby ground. For TEM propagation, the per-unit-length parameters can be determined using a 2D static field solver. For the static field solution, the ground can be moved farther and farther away from the conductors until its size and location no longer affect the solution. The per-unit-length parameters calculated with ground essentially at infinity and (25) have been used to determine the imbalance factors by a number of researchers and successfully were applied to modeling the radiated emissions of a wide variety of structures [4]–[17].

However, the AM currents are not TEM and do not satisfy the telegrapher's equations; and it is reasonable to expect that the size and orientation of the conductor on the other wing of the antenna, can have an effect on the current division factor. To illustrate this point, we drive a two-conductor TL with a quasi-static voltage source

against another conductor, as shown in **Error! Reference source not found.**. The arrows in Fig.1.17 represent the resulting electric field distribution. If the left side conductor is bent upwards, as indicated in **Error! Reference source not found.**, the field distribution near the two-conductor TL changes causing slightly more AM current to flow on the upper conductor of the TL.

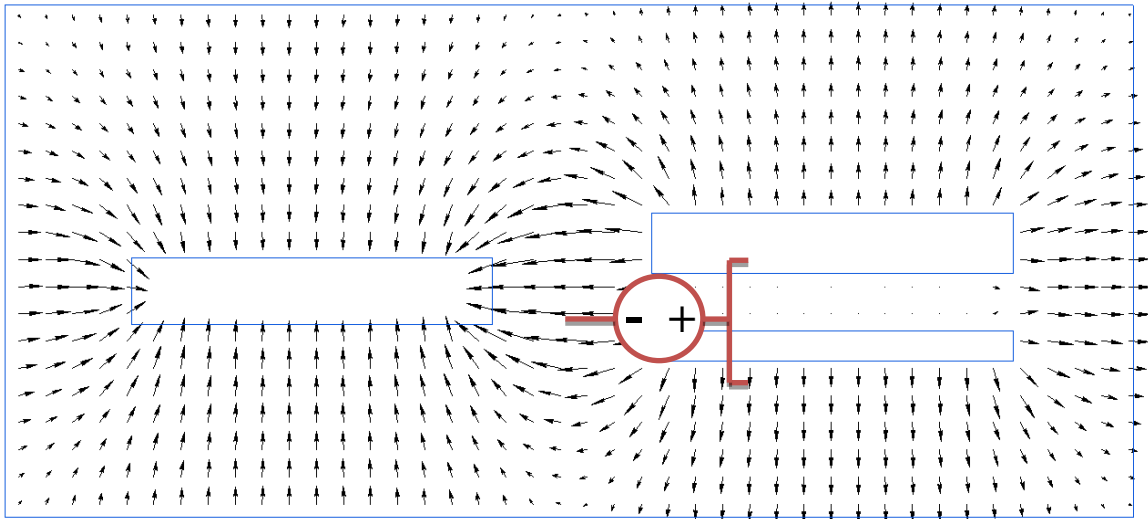


Fig.1. 17. Illustration of electric field distribution resulted from a quasi-static source driving a two-conductor transmission line relative to another wire.

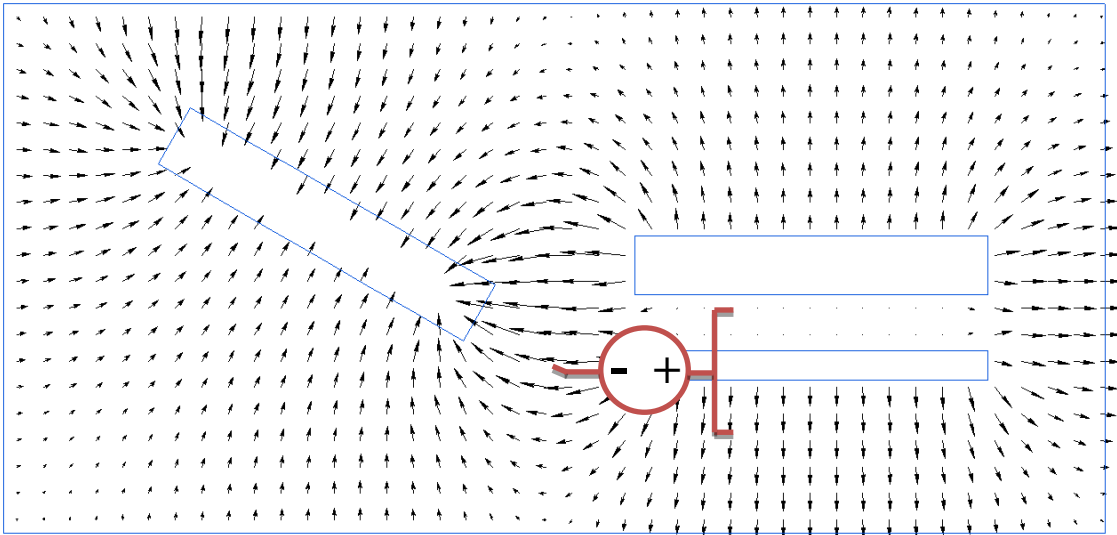


Fig.1. 18. Illustration of electric field distribution resulted from a quasi-static source driving a two-conductor transmission line relative to another angled wire.

However, even though current division factor calculated using (23) is not mathematically exact, it is a very good approximation of the actual current division factor for most radiating structures of practical interest. This is because, for most monopole or dipole antenna structures, the geometry on one side of the antenna has very little effect on the field distribution near the conductor(s) on the other side. The following section illustrates this using three example structures.

1.5 Example Calculations

To examine how much the current division factor on one half of a dipole antenna is affected by the geometry of the other side, the current division factors of some example structures were calculated using a 3D full-wave field solver and compared to calculations made using a 2D static field solver. The 2D static field solver we used was QuickField Students' version [18], which employs a Finite Element Method. The 3D full wave solver we used was FEKO [19], which is a Method of Moments code.

1.5.1 Description of the Example Structures

The first structure is shown in Fig.1. 19. A TL is formed by two wire conductors with circular cross-sections that have radii $R_1=1\text{ mm}$ and $R_2=2\text{ mm}$. The wires are 12 mm apart. This TL is driven by an AM source relative to another wire conductor with radius $R_3=5\text{ mm}$. The lengths of all the wire conductors are 500 mm.

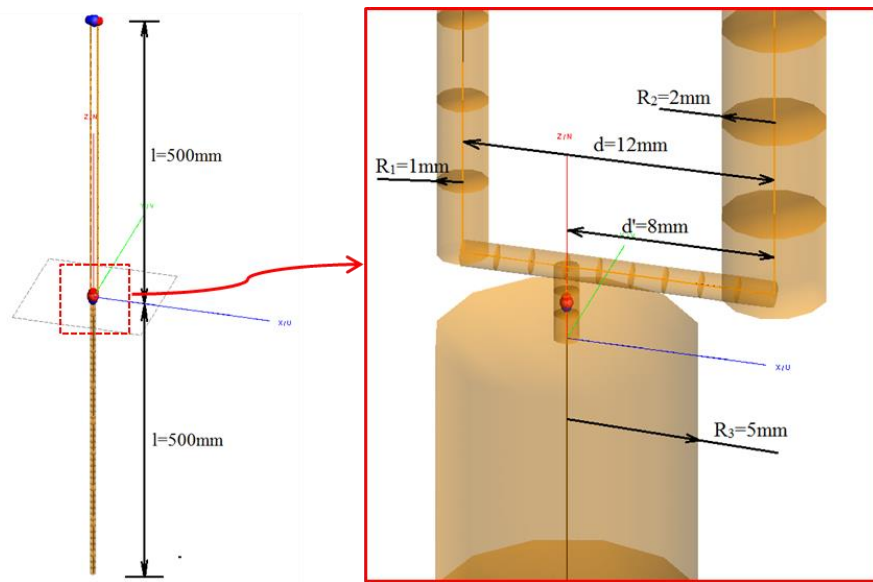


Fig.1. 19. Example Structure 1.

The second structure is shown in Fig.1. 20. The same TL as that in Structure 1 is driven by the same AM source. On the other side of the AM voltage source, instead of a wire, there is a metal sheet that is perpendicular to the TL. The metal sheet is connected to the AM source at the center of one edge and extends to the right side. This structure is intended to bias the current division factor by making it easier for current to flow on the right-side wire of the TL rather than the left-side wire.

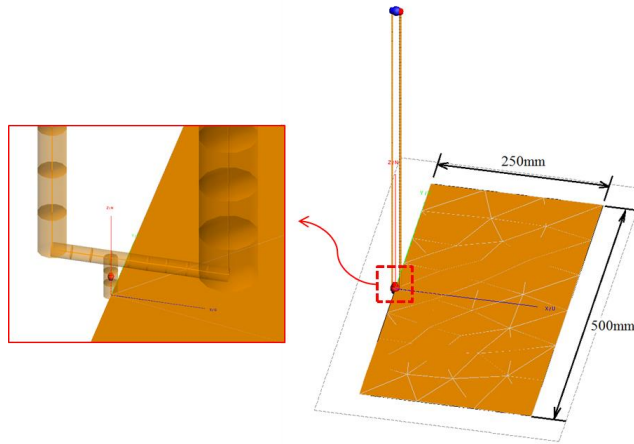


Fig.1. 20. Example structure 2.

The third structure is similar to Structure 2 except the metal sheet is flipped to the left side, so that it favors current flowing on the left-side wire of the TL, as shown in Fig.1. 21.

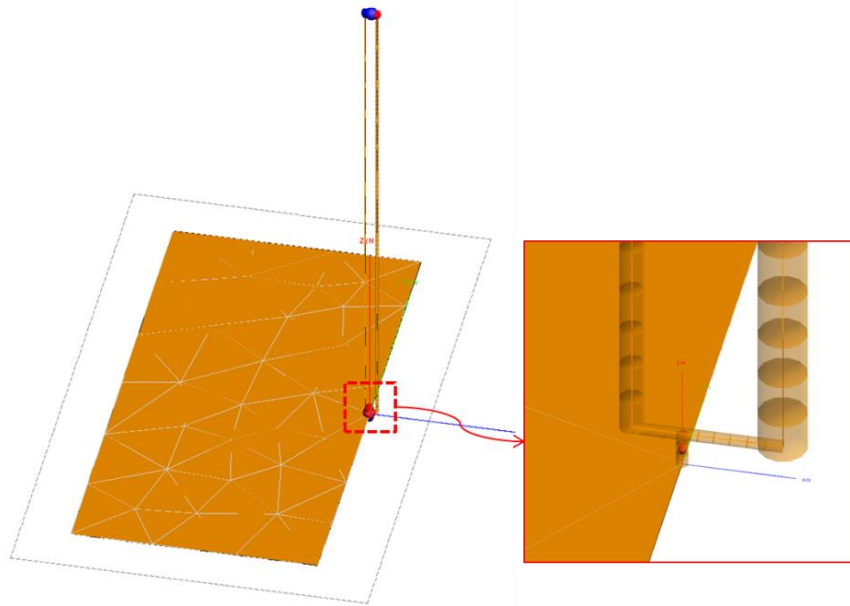


Fig.1. 21. Example structure 3.

1.5.2 Calculation Results

Fig.1. 222 shows the calculated current division factor obtained using the 2D static field solver and 3D full-wave code over the frequency range from 30 MHz to 200 MHz.

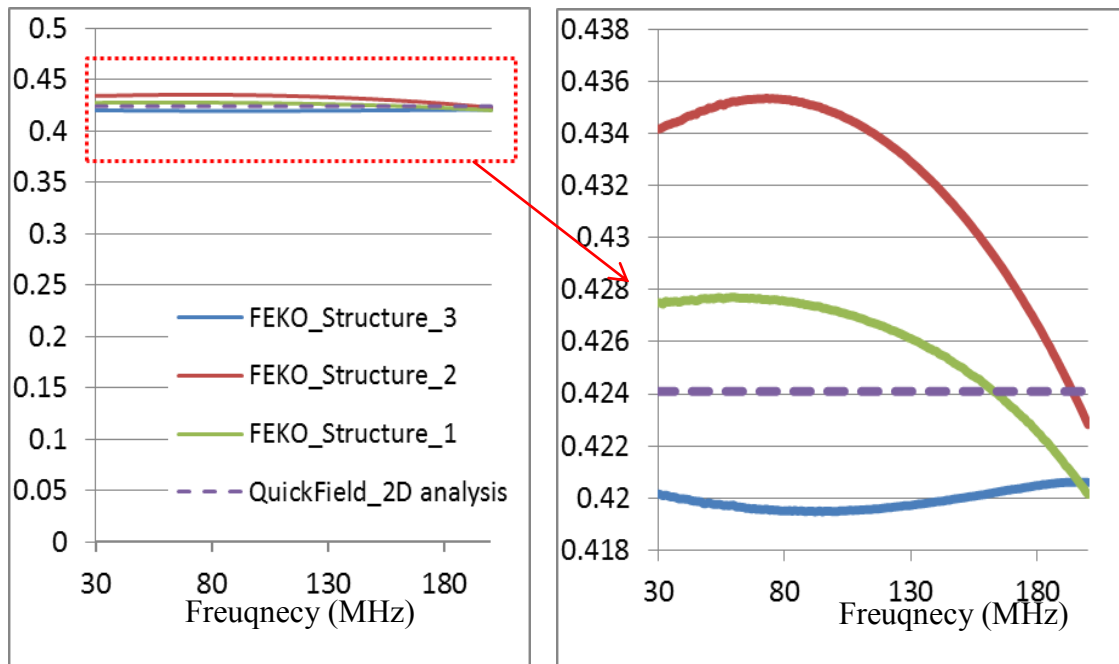


Fig.1. 222. Current division factor calculation result over 30MHz to 200MHz.

In Fig.1. 222, the three solid lines are current division factors calculated using FEKO, for Structures 1, 2 and 3. All of them are curved over frequency, which means the actual current division factor is a function of frequency. The relative positions of these three solid lines are consistent with our expectation that the conductor on one wing of the antenna will affect the current distribution between two conductors on the other wing. However, for all three structures over the full frequency range, the biggest current division factor we obtained was 0.435 and the smallest was 0.419, which is less than a 4% difference. Since the asymmetry in these examples was greater than those which

would be encountered in most practical situations, 2D static field solvers will generally provide a fairly accurate estimate of the current division factor.

1.6 Conclusion

The imbalance difference theory as applied to radiated emission modeling has been derived rigorously without making any assumptions related to TEM propagation of the antenna-mode signals. The relationship between differential-mode voltage and antenna-mode voltage at points where there is a change in electrical balance is precisely described by (24) as long as the differential-mode propagation is TEM and the current division factor, h , represents the actual division of antenna-mode current on the transmission line.

The second part of this paper demonstrates that the division of antenna-mode current on one half of a radiating dipole structure is relatively independent of the geometry of the other half. A simple 2D analysis of the cross-section of the transmission line provides an excellent approximation of the actual current division factor.

References

- [1] C. R. Paul, "A comparison of the contributions of common-mode and differential-mode currents in radiated emissions," *IEEE Trans. Electromagn. Compat.*, vol. 31, no. 2, pp. 189–193, May 1989.
- [2] T. H. Hubing and J. F. Kaufman, "Modeling the electromagnetic radiation from electrically small table-top products," *IEEE Trans. Electromagn. Compat.*, vol. 31, no. 1, pp. 74–84, 1989.

- [3] T. Watanabe, O. Wada, T. Miyashita, and R. Koga, "Common-Mode-Current Generation Caused by Difference of Unbalance of Transmission Lines on a Printed Circuit Board with Narrow Ground Pattern," *IEICE Trans. Commun.*, vol. E83-B, no. 3, pp. 593–599, Mar. 2000.
- [4] T. Watanabe, H. Fujihara, O. Wada, R. Koga, and Y. Kami, "A Prediction Method of Common-Mode Excitation on a Printed Circuit Board Having a Signal Trace near the Ground Edge," *IEICE Trans. Commun.*, vol. E87-B, no. 8, pp. 2327–2334, Aug. 2004.
- [5] T. Watanabe, O. Wada, Y. Toyota, and R. Koga, "Estimation of common-mode EMI caused by a signal line in the vicinity of ground edge on a PCB," in *IEEE International Symposium on Electromagnetic Compatibility*, 2002, vol. 1, pp. 113–118.
- [6] T. Watanabe, M. Kishimoto, S. Matsunaga, T. Tanimoto, R. Koga, O. Wada, and A. Namba, "Equivalence of two calculation methods for common-mode excitation on a printed circuit board with narrow ground plane," in *2003 IEEE Symposium on Electromagnetic Compatibility. Symposium Record (Cat. No.03CH37446)*, 2003, vol. 1, pp. 22–27.
- [7] O. Wada, "Modeling and simulation of unintended electromagnetic emission from digital circuits," *Electron. Commun. Japan (Part I Commun.)*, vol. 87, no. 8, pp. 38–46, Aug. 2004.
- [8] Y. Toyota, A. Sadatoshi, T. Watanabe, K. Iokibe, R. Koga, and O. Wada, "Prediction of electromagnetic emissions from PCBs with interconnections through common-mode antenna model," in *2007 18th International Zurich Symposium on Electromagnetic Compatibility*, 2007, pp. 107–110.
- [9] Y. Toyota, T. Matsushima, K. Iokibe, R. Koga, and T. Watanabe, "Experimental validation of imbalance difference model to estimate common-mode excitation in PCBs," in *2008 IEEE International Symposium on Electromagnetic Compatibility*, 2008, pp. 1–6.
- [10] T. Matsushima, T. Watanabe, Y. Toyota, R. Koga, and O. Wada, "Evaluation of EMI Reduction Effect of Guard Traces Based on Imbalance Difference Model," *IEICE Trans. Commun.*, vol. E92-B, no. 6, pp. 2193–2200, Jun. 2009.
- [11] T. Matsushima, T. Watanabe, Y. Toyota, R. Koga, and O. Wada, "Increase of Common-Mode Radiation due to Guard Trace Voltage and Determination of Effective Via-Location," *IEICE Trans. Commun.*, vol. E92-B, no. 6, pp. 1929–1936, Jun. 2009.

- [12] C. Su and T. H. Hubing, "Imbalance Difference Model for Common-Mode Radiation From Printed Circuit Boards," *IEEE Trans. Electromagn. Compat.*, vol. 53, no. 1, pp. 150–156, Feb. 2011.
- [13] K. Sejima, Y. Toyota, K. Iokibe, L. R. Koga, and T. Watanabe, "Experimental model validation of mode-conversion sources introduced to modal equivalent circuit," *2012 IEEE Int. Symp. Electromagn. Compat.*, pp. 492–497, Aug. 2012.
- [14] T. Matsushima, O. Wada, T. Watanabe, Y. Toyota, and L. R. Koga, "Verification of common-mode-current prediction method based on imbalance difference model for single-channel differential signaling system," in *2012 Asia-Pacific Symposium on Electromagnetic Compatibility*, 2012, vol. 2, pp. 409–412.
- [15] A. Sugiura and Y. Kami, "Generation and Propagation of Common-Mode Currents in a Balanced Two-Conductor Line," *IEEE Trans. Electromagn. Compat.*, vol. 54, no. 2, pp. 466–473, Apr. 2012.
- [16] H. Al-Rubaye, K. Pararajasingam, and M. Kane, "Estimating radiated emissions from microstrip transmission lines based on the imbalance model," in *2012 IEEE Electrical Design of Advanced Packaging and Systems Symposium (EDAPS)*, 2012, pp. 93–96.
- [17] H. Kwak and T. H. Hubing, "Investigation of the imbalance difference model and its application to various circuit board and cable geometries," in *2012 IEEE International Symposium on Electromagnetic Compatibility*, 2012, pp. 273–278.
- [18] "QuickField Student Edition." [Online]. Available: http://www.quickfield.com/free_soft.htm. [Accessed: 25-Jun-2014].
- [19] *FEKO User 's Manual*, Suite 6.2. 2013.

CHAPTER TWO

MODELING THE CONVERSION BETWEEN DIFFERENTIAL MODE AND COMMON MODE PROPAGATION IN TRANSMISSION LINES

Abstract

The imbalance difference theory describes a method for calculating the coupling between differential mode signals and common mode signals due to changes in electrical balance on a transmission line. It provides both physical insight and a simple technique for modeling the conversions between two modes. This paper provides a rigorous development of the theory for three-conductor transmission lines and derives expressions for the mode conversion impedances. The conversion impedances account for the energy converted from one mode to the other, and are essential for modeling the conversion between the two modes when they are strongly coupled.

2.1 Introduction

High-speed digital signals are often transmitted from one point to another as differential signals on balanced two-conductor transmission lines. The balanced

conductors generally have identical cross-sections and have the same electrical impedance to any other conductors in the system. In order to help maintain constant impedances, these two conductors are often located near a third reference conductor (typically labeled “ground”). The differential-mode (DM) currents on the two signal conductors are equal in magnitude and flow in opposite directions everywhere along the transmission line. No current is intended to flow on the reference conductor; but discontinuities in the electrical balance of the two-conductor transmission line can cause energy to be converted from the differential-mode to common-mode (CM) noise. One problem resulted from this conversion is that it reduces the amount of signal power available at the far end of the line. Another issue that is generally of far greater importance is that even small amounts of CM noise can contribute significantly to radiated emissions at the frequencies typically associated with high-speed digital signaling [1]. However, not all CM currents radiate, for example, if the CM current returns by an adjacent reference conductor, the total effect of radiation will be negligible. In a recently published paper by the author [xxx], we distinguished the CM signals that radiate as antenna-mode (AM), and the CM signals we will refer to in the rest of the paper means those with TEM propagation and can be analyzed with transmission line theory.

The DM and CM signals of TLs, also known as odd-mode and even-mode, have been studied in papers [2]–[8]. These papers focus on the description of the modes in microwave engineering point of view. A specific PCB and trace configuration was

studied in paper [9], and several balanced TL configurations were studied in papers [10]–[12].

In 2000, Watanabe introduced the concept of *electrical balance* and *imbalance factor* for a transmission line (TL). He demonstrated that the generation of CM current from DM signals is caused by the change of the electrical balance of the TL [13]. In that paper, CM currents were calculated by placing ideal CM voltage sources at locations where electrical balance changed. This concept, which has come to be known as the imbalance difference theory (IDT) provides great insight to the conversion mechanism between DM and CM, and it has been successfully used to model a number of radiated emission problems [14]–[25] and a board-level CM signal reduction problem [26].

When it was introduced, the IDT was derived using concepts from multi-conductor transmission line theory that inherently assume that both the DM and the CM signals propagate in TEM mode. However, in the radiated emission examples to which it was applied, the common mode signals were not TEM. A rigorous derivation of IDT for the radiation case is provided in another paper by the authors [xx]. This paper rigorously derives the IDT equations applicable to two-conductor transmission lines routed with a reference conductor. Examples of this geometry include signal trace pairs routed over a circuit board reference plane and shielded twisted-wire pairs. The results include expressions for the conversion impedances associated with DM-to-CM and CM-to-DM coupling in these configurations.

A DM-CM conversion model was presented in paper [27], but it was relied on the measurement of S parameters and only balanced transmission lines were discussed. The

energy conversion between DM and CM was studied using IDT by [28]. In comparison, we propose the concept of conversion impedances into the existing models, which can show the impact of mode-conversion to the original circuits in a more intuitive way. We will also present a logical derivation of the desirable definitions of DM and CM signals.

2.2 Definition of Differential Mode and Common Mode Signals

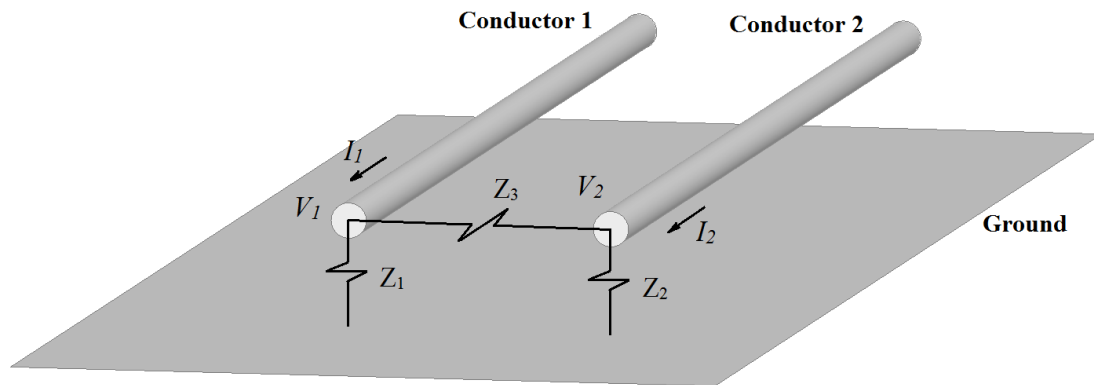


Fig.2.23. A two-conductor TL above a reference plane with matching termination.

Consider the pair of wires routed above a reference plane illustrated in Fig.2.1. Viewing the two conductors and the reference plane as a three-conductor transmission line, Z_1 , Z_2 and Z_3 are the impedances that are required to match all forward-propagating modes at the termination. The currents on conductors 1 and 2 are I_1 and I_2 , respectively. V_1 and V_2 are the voltages between each conductor and the reference plane.

If the signal is propagating on the wire pair, it is inconvenient to view the propagating modes in terms of V_1 , I_1 and V_2 , I_2 . Instead, it is preferable to view the two independent propagation modes in terms of V_{DM} , I_{DM} and V_{CM} , I_{CM} . For a TEM wave

propagating along the transmission line in the forward direction (i.e. towards the termination), we define the DM voltage as the voltage difference between two conductors,

$$V_{DM}^+ = V_1^+ - V_2^+ . \quad (24)$$

The CM current is defined as the total current that flows on both conductors,

$$I_{CM}^+ = I_1^+ + I_2^+ . \quad (25)$$

If DM and CM are mutually independent, the voltage and current associated with each mode are related by their own characteristic impedances:

$$V_{DM}^+ = Z_{DM} I_{DM}^+ , \quad (26)$$

$$V_{CM}^+ = Z_{CM} I_{CM}^+ . \quad (27)$$

For a pure DM signal arriving at the termination, the CM current and voltage are zero, and the DM current flows from one wire conductor to the other. This current flows through Z_3 and the series combination of Z_1 and Z_2 , so the DM impedance is:

$$Z_{DM} = Z_3 \parallel (Z_1 + Z_2) . \quad (28)$$

Combining equations (1), (3) and (5), we obtain the definition for I_{DM}^+ necessary to ensure the independence of the DM and CM propagating modes,

$$I_{DM}^+ = \frac{Z_1}{Z_1 + Z_2} \cdot I_1^+ - \frac{1}{Z_1} \cdot \frac{Z_2}{Z_1 + Z_2} \cdot I_2^+ . \quad (29)$$

For a pure CM signal arriving at the termination, the DM voltage and current are zero. Since both conductors have the same voltage, CM current flows from both conductors through the parallel combination of Z_1 and Z_2 to the reference conductor, so the CM impedance is:

$$Z_{CM} = Z_1 \parallel Z_2 . \quad (30)$$

Combining equations (2), (4) and (7) yields the definition for V_{CM} :

$$V_{CM}^+ = \frac{Z_2}{Z_1 + Z_2} V_1^+ - \frac{1}{Z_1} \frac{1}{Z_2} V_2^+ . \quad (31)$$

For a backward propagating wave, we can define the DM and CM propagating modes similarly:

$$V_{DM}^- = V_1^- - V_2^- , \quad (32)$$

$$I_{CM}^- = I_1^- + I_2^- , \quad (33)$$

$$I_{DM}^- = \frac{Z_1}{Z_1 + Z_2} \cdot I_1^- - \frac{1}{Z_1} \frac{1}{Z_2} \cdot I_2^- , \quad (34)$$

$$V_{CM}^- = \frac{Z_2}{Z_1 + Z_2} V_1^- - \frac{1}{Z_1} \frac{1}{Z_2} V_2^- , \quad (35)$$

Combining both the forward and backward wave, i.e., combining equations(26), (27),(29) and (31) with the corresponding equations (32),(33),(34), and (35), we have:

$$V_{DM} = V_{DM}^+ + V_{DM}^- = (V_1^+ + V_1^-) - (V_2^+ + V_2^-) = V_1 - V_2 , \quad (36)$$

$$I_{CM} = I_{CM}^+ - I_{CM}^- = (I_1^+ - I_1^-) + (I_2^+ - I_2^-) = I_1 + I_2 , \quad (37)$$

$$V_{CM} = V_{CM}^+ + V_{CM}^- = \frac{Z_2}{Z_1 + Z_2} (V_1^+ + V_1^-) + \frac{Z_1}{Z_1 + Z_2} (V_1^+ + V_1^-) = \frac{Z_2}{Z_1 + Z_2} V_1 + \frac{Z_1}{Z_1 + Z_2} V_2, \quad (38)$$

$$I_{DM} = I_{DM}^+ - I_{DM}^- = \frac{Z_1}{Z_1 + Z_2} (I_1^+ - I_1^-) - \frac{Z_1}{Z_1 + Z_2} (I_2^+ - I_2^-) = \frac{Z_2}{Z_1 + Z_2} I_1 - \frac{Z_1}{Z_1 + Z_2} I_2. \quad (39)$$

If we define

$$\frac{Z_2}{Z_1 + Z_2} \equiv h, \quad (40)$$

then the definition of DM and CM signals can be rewritten in the following form:

$$V_{DM} = V_1 - V_2, \quad (41)$$

$$I_{DM} = (1-h)I_1 - h \cdot I_2, \quad (42)$$

$$V_{CM} = h \cdot V_1 + (1-h) \cdot V_2, \quad (43)$$

$$I_{CM} = I_1 + I_2. \quad (44)$$

In the appendix, it is shown that the factor “ h ” defined in Equation(40) with impedances is the same as the imbalance factor defined by Watanabe in [13] with capacitances or inductances. The definitions of DM and CM signals are also consistent.

When the two-conductor TL is perfectly balanced, i.e. $Z_1=Z_2$, the definitions of DM and CM signals become:

$$\begin{aligned} V_{DM} &= V_1 - V_2, \\ V_{CM} &= (V_1 + V_2) / 2, \\ I_{DM} &= (I_1 - I_2) / 2, \\ I_{CM} &= I_1 + I_2. \end{aligned} \quad (45)$$

2.3 Conversion between Differential Mode and Common Mode

By definition, as long as the electrical balance does not change along the TL, the DM and CM signals propagate independently. However, as indicated by equations (19) and (20), any change in the electrical balance along the line will cause a discontinuity in the values of I_{DM} and V_{CM} .

Fig.2.24 shows a two-conductor TL above a reference plane that exhibits a change in the electrical balance. The matching impedances for the left section and right section of the TL are Z_{1L}, Z_{2L}, Z_{3L} and Z_{1R}, Z_{2R}, Z_{3R} respectively.

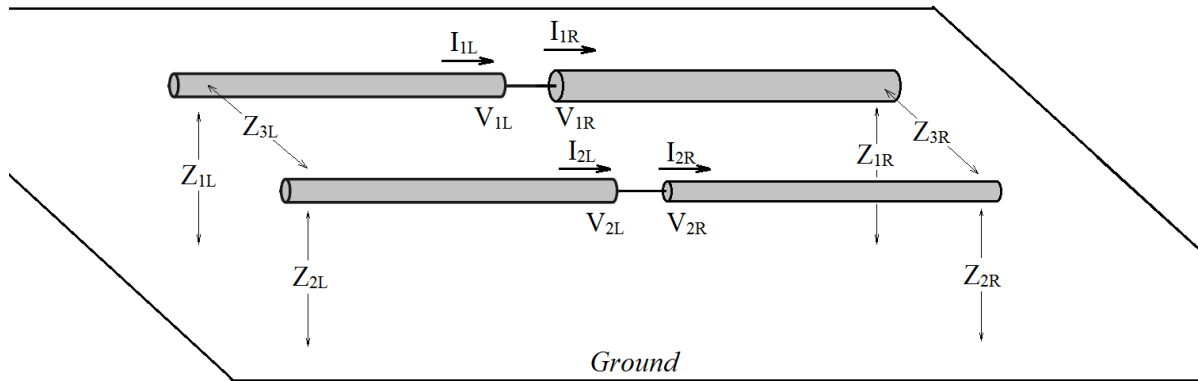


Fig.2.24. Two-conductor TL with a discontinuity of electrical balance above a reference plane.

At the interface where the electrical balance changes, the boundary condition requires the voltages and the currents on each conductor to be continuous, i.e.

$$\begin{aligned}
 V_{1L} &= V_1 & V_1, \\
 V_{2L} &= V_2 & V_2, \\
 I_{1L} &= I_1 & I_1, \\
 I_{2L} &= I_2 & I_2.
 \end{aligned}
 \tag{46}$$

From (18) and (21), it is apparent that the DM voltage and CM current are also continuous at the interface,

$$V_{DM_L} = V_1 - V_2 = V_{DM_R} \equiv V_{DM} , \quad (47)$$

$$I_{CM_L} = I_1 + I_2 = I_{CM_R} \equiv I_{CM} . \quad (48)$$

Since the imbalance factors of the left section and right section are different,

$$h_L = \frac{Z_{2L}}{Z_{1L} +} , \quad (49)$$

$$h_R = \frac{Z_{2R}}{Z_{1R} +} , \quad (50)$$

According to (42) and (43), the CM voltages and DM currents are different for each section of the TL,

$$\begin{aligned} V_{CM_L} &= h_L \cdot V_1 + (1 - h_L) \cdot V_2, \\ V_{CM_R} &= h_R \cdot V_1 + (1 - h_R) \cdot V_2, \\ I_{DM_L} &= (1 - h_L)I_1 - h_L \cdot I_2, \\ I_{DM_R} &= (1 - h_R)I_1 - h_R \cdot I_2. \end{aligned} \quad (51)$$

The change in the CM voltage and DM current across the interface can be expressed as:

$$\Delta V_{CM} = V_{CM_L} - V_{CM_R} = \Delta h \cdot (V_1 - V_2) = \Delta h \cdot V_{DM} , \quad (52)$$

$$\Delta I_{DM} = I_{DM_L} - I_{DM_R} = \Delta h \cdot (I_1 + I_2) = -\Delta h \cdot I_{CM} . \quad (53)$$

Equations (52) and (53) indicate that a change in the electrical balance along a transmission line results in a virtual CM voltage, ΔV_{CM} , that drives one side of the TL relative to the other side. ΔV_{CM} is proportional to the DM voltage at the interface and the change of the electrical balance. There will also be a virtual DM current, ΔI_{DM} , that flows from one conductor to the other at the interface. This DM current is virtual, because no actual electric charge moves from one conductor to the other. I_{DM} takes on a new value due to the fact that it is defined differently in terms of I_1 and I_2 , which are constant across the interface. ΔI_{DM} is proportional to the CM current at the interface and the change of the electrical balance.

2.4 Models of the Differential Mode and Common Mode Conversion

For a two-conductor TL above a reference plane, we can decompose any signals into two independent propagating modes, DM and CM. As shown in Fig.2.25, the upper TL circuit represents only the DM propagation and the lower TL circuit represents only the CM propagation.

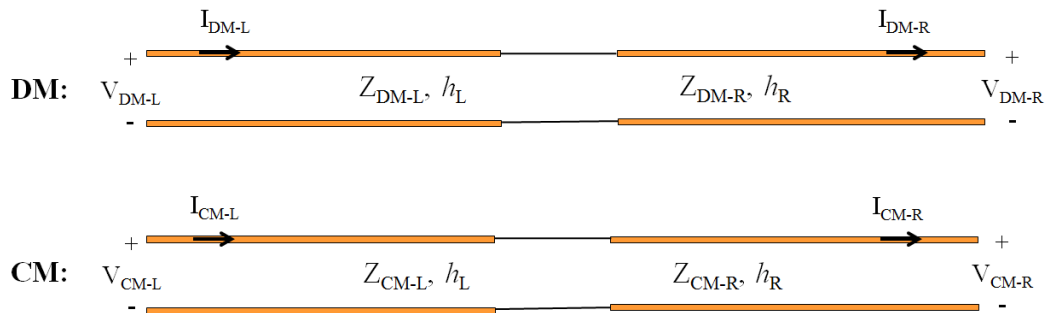


Fig.2.25. Decomposition of the original circuit into DM and CM propagation.

2.4.1 Model of DM-to-CM Conversion

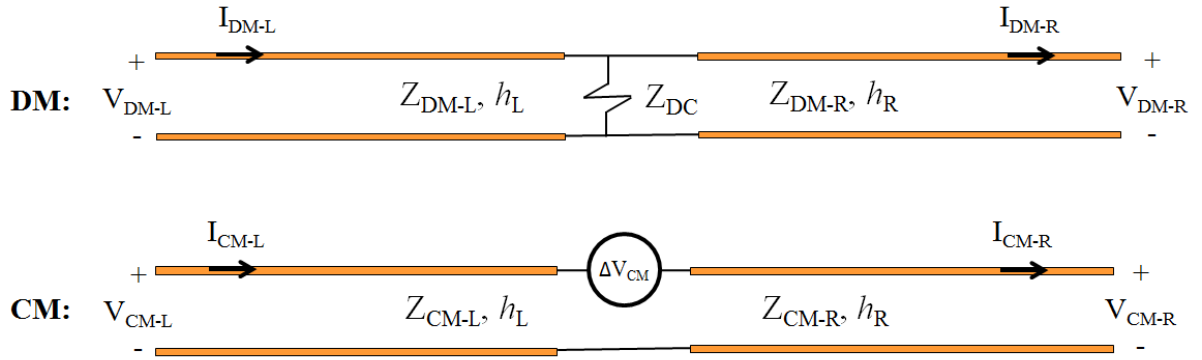


Fig.2.26. Equivalent model for DM-to-CM conversion.

Consider a DM signal propagating on the DM TL of Fig.2.3. From (52), it is clear that the DM voltage at the interface will generate a CM voltage difference, ΔV_{CM} . This can be represented as an ideal voltage source in the CM circuit as shown in the lower part of Fig.2.26,

$$\Delta V_{CM} = V_{DM} \cdot \Delta h . \quad (54)$$

The ΔV_{CM} will drive the CM circuit and generate a CM current, the impedance that ΔV_{CM} sees is the series combination of the input impedances of each side of the TL in the CM circuit, so the generated CM current will be:

$$I_{CM} = \frac{\Delta V_{CM}}{Z_{CM-L} + Z_{CM-R}} = \frac{V_{DM} \cdot \Delta h}{Z_{CM-L} + Z_{CM-R}} . \quad (54)$$

According to Equation (53), this I_{CM} at the interface will produce a DM current,

$$\Delta I_{DM} = \Delta h \cdot I_{CM} = \frac{V_{DM} \cdot (\Delta h)^2}{Z_{CM-L} + Z_{CM-R}} . \quad (55)$$

ΔI_{DM} can be regarded as the effect of the DM-CM conversion on the original DM signal. It can be represented by a shunt impedance in the DM circuit as shown in Fig.2.26. Here, we will refer to it as the DM-to-CM conversion impedance, Z_{DC} :

$$Z_{DC} = \frac{V_{DM}}{\Delta I_{DM}} = \left(\frac{1}{\Delta h} \right)^2 [Z_{CM-L} + Z_{CM-R}]. \quad (56)$$

Z_{DC} is the loading effect on the DM signal that accounts for the energy conversion from DM to CM. If the coupling is weak (i.e. Δh is very small or the CM impedances are much bigger than the DM impedances), then Z_{DC} is much bigger than Z_{DM} , and it can be neglected. However, if the values of the CM impedances are comparable to the DM impedances and the change of electrical balance is significant at the interface, then Z_{DC} must be considered in order to accurately calculate the DM voltage at the interface.

2.4.2 Model of CM-to-DM Conversion

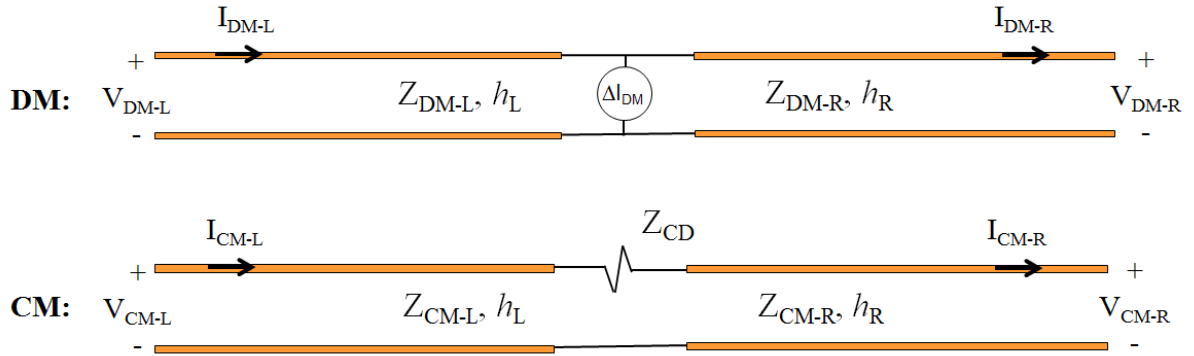


Fig.2.27. Equivalent model for CM-to-DM conversion.

Equation (53) points out that CM current will generate DM current, ΔI_{DM} , at the interface where the electrical balance changes, This can be modeled as an ideal current source in the DM circuit, as shown in the upper part of Fig.2.27,

$$\Delta I_{DM} = I_{CM} \cdot \Delta h. \quad (56)$$

In the DM circuit, ΔI_{DM} will flow through the parallel combination of the input impedances of both sides of the TL and generate a DM voltage at the interface:

$$V_{DM} = \Delta I_{DM} \cdot (Z_{DM-L} \parallel Z_{DM-R}) = I_{CM} \cdot \Delta h \cdot (Z_{DM-L} \parallel Z_{DM-R}). \quad (56)$$

According to Equation (52), this DM voltage will cause a change in CM voltage, ΔV_{CM} , at the interface,

$$\Delta V_{CM} = h \cdot V_{DM} = I_{CM} \cdot (\Delta h)^2 \cdot (Z_{DM-L} \parallel Z_{DM-R}). \quad (57)$$

ΔV_{CM} can be regarded as the effect of the CM-DM conversion on the original CM circuit. It can be represented by a series impedance in the CM circuit, as shown in the lower part of Fig.2.27. Here, it is referred to as the CM-DM conversion impedance, Z_{CD} :

$$Z_{CD} = \frac{\Delta V_{CM}}{I_{CM}} = (\Delta h)^2 \cdot (Z_{DM-L} \parallel Z_{DM-R}). \quad (57)$$

Z_{CD} represents the loading effect on a CM signal that accounts for the energy conversion from CM to DM. Like Z_{DC} , Z_{CD} plays an important role if the two modes are strongly coupled, and it is negligible if the conversion is weak.

2.5 Example

This section demonstrates the implementation of IDT on a multi-conductor transmission line structure where both the DM and CM signals exhibit TEM propagation and the coupling between the two modes is strong. As shown in **Error! Reference source not found.**, two cylindrical conductors of different radii form a two-conductor TL

enclosed by a reference conductor. The total length of the TL is 600 mm. In the middle of the TL, the diameter of the two TL conductors abruptly changes, so that the electric balance is changed while the DM characteristic impedance stays the same. Near the left end of the TL, there is a 2-volt DM voltage source with 50- internal impedance that drives the two conductors. The three-conductor system is perfectly matched at each end.

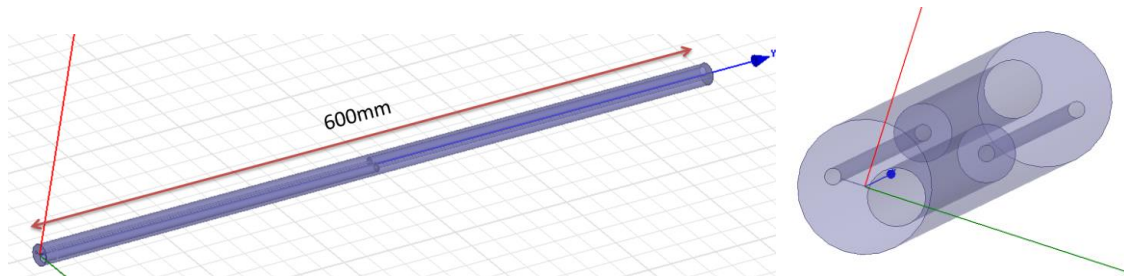


Fig.2. 28. Example structure in 3D views.

The dimensions of the cross-section of the structure are shown in Fig.2.7. The excitation frequency is 1GHz.

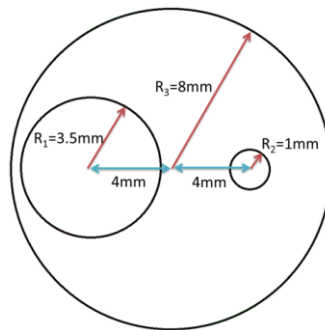


Fig.2. 29. The cross-section of the two-conductor transmission line and the reference conductor.

2.5.1 Calculation by Imbalance Difference Theory

The excitation is purely differential, but we expect to find power propagating in both modes due to the mode conversion that occurs at the middle of the line. To solve for the signal amplitudes in each mode using the imbalance difference theory, the imbalance factor on each side was calculated by per-unit-length capacitances using a 2D static field

solver, ATLC2 [29]. The results are shown in Table 2.1. C_{11} , C_{22} and C_{33} are the per-unit-length capacitances illustrated schematically in Fig.2. 30.

Table 2.1. Capacitances calculated by ATLC2

$C_{11}+C_{33}$	$C_{22}+C_{33}$	$C_{11}+C_{22}$	C_{11}	C_{22}	C_{33}
150.621 pF/m	33.91 pF/m	164.96 pF/m	140.84 pF/m	24.12 pF/m	9.78 pF/m

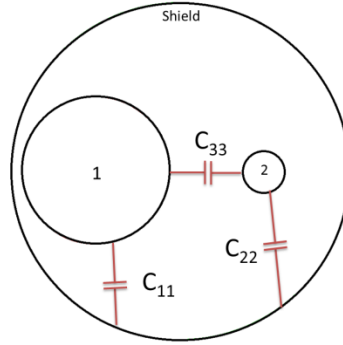


Fig.2. 30. Per-unit-length capacitances between conductors.

From the data in Table 2.1, the imbalance factor of the two-conductor transmission line on one side of the discontinuity is:

$$h = \frac{C_{11}}{C_{11} + C_{22}} = 0.8538 . \quad (57)$$

On the other side of the discontinuity, because the conductors have a similar cross-section with switched positions of conductor 1 and conductor 2, the imbalance factor is equal to one minus the imbalance factor on the first side. The change in the imbalance factor across the discontinuity is therefore,

$$\Delta h = h - (1 - h) = 0.7075 . \quad (57)$$

The per-unit-length capacitances associated with the DM and CM propagation are,

$$C_{DM} = C_{33} + C_{11} \cdot C_{22} / (C_{11} + C_{22}) = 30.38 pF / m , \quad (57)$$

$$C_{CM} = C_{11} + C_{22} = 164.86 pF / m . \quad (57)$$

Since both modes exhibit TEM propagation, the characteristic impedances of each mode are:

$$Z_{DM} = \frac{1}{u \cdot C_{DM}} = 109.73 \text{ ohm} , \quad (57)$$

$$Z_{CM} = \frac{1}{u \cdot C_{CM}} = 20.21 \text{ ohm} , \quad (57)$$

where u is the velocity of propagation. According to (56), the conversion impedance is,

$$Z_{DC} = \frac{V_{DM}}{\Delta I_{DM}} = \left(\frac{1}{2} \right)^2 [Z_{CM-L} + Z_{CM-R}] = 80.73 \text{ ohm} . \quad (57)$$

In the DM circuit as represented in Fig.2.26, the impedance at the interface looking towards the right will be,

$$Z_{middle} = Z_{DC} \parallel Z_{DM} = 45.51 \text{ ohm} . \quad (57)$$

The impedance at the source looking to the right will be,

$$Z_{source-right} = Z_{DM} \cdot \frac{Z_{middle} + j \cdot Z_{DM} \cdot \tan \beta l}{Z_{DM} + j \cdot Z_{middle} \cdot \tan \beta l} = 46.51 \text{ ohm} \quad (57)$$

Therefore, the total impedance the DM source sees is,

$$Z_{input} = Z_{source-right} \parallel Z_{DM} = 32.66 \text{ ohm} , \quad (57)$$

and the DM voltage across two conductors at the source is,

$$V_{DM@source} = \text{source} \cdot \frac{Z_{input}}{Z_s + Z_{input}} = 0.7903 \text{ V} . \quad (57)$$

At the interface, the voltage propagating towards the right (positive) direction will be,

$$V_0^+ = \frac{V_{DM@source}}{(e^{j\beta l} + \Gamma_{mid} \cdot e^{-j\beta l})} = 1.33 \text{ V} . \quad (57)$$

The reflection coefficient at the interface looking from the left is,

$$\Gamma_{middle} = \frac{Z_{middle} - Z_{DM}}{Z_{middle} + Z_{DM}} = -0.4046 . \quad (57)$$

So the DM voltage at the interface is,

$$V_{DM} = V^+ + V^- \cdot \Gamma_{middle} = 0.79 \text{ V} . \quad (57)$$

Then based on the IDT, the equivalent CM voltage source amplitude will be,

$$\Delta V_{CM} = V_{DM} \cdot \Delta h = 0.56 \text{ V} , \quad (57)$$

and the CM current will be,

$$I_{CM} = \frac{\Delta V_{CM}}{2 \cdot Z_{CM}} = 13.8 \text{ mA} . \quad (57)$$

Note that the left section of the TL is no longer impedance matched to the right section due to the mode conversion resistance. This will create a standing wave in the left section with standing wave ratio of,

$$SWR = \frac{1 + |\Gamma_{middle}|}{1 - |\Gamma_{middle}|} = 2.36 . \quad (57)$$

For the purpose of comparison, if we neglected to account for the conversion impedance in this example, then the DM voltage at the middle of the TL in **Error! Reference source not found.** would have been the same as that at the source:

$$V_{DM}' = V_{source} \cdot \frac{Z_{DM} / 2}{Z_s + Z_{DM} / 2} = 1.0464 . \quad (57)$$

In this case, the calculated CM current would have been,

$$I_{CM}' = \frac{\Delta V_{CM}}{2 \cdot Z_{CM}} = \frac{V_{DM} \cdot \Delta h}{CM} = 18.3 \text{ mA} , \quad (57)$$

or 33% higher than the correct value.

2.5.2 Calculation by 3D full wave simulation

A full wave simulation code, HFSS [30], was used to calculate the currents in the Fig.2.6 structure at 1GHz. From these currents, the DM and CM currents along were determined by (19) and (21). They are plotted in Fig.2. 31. The solid line is the CM current, which is constant along the TL. The dashed line is the DM current, it exhibits a standing wave pattern on the left half and is constant on the right. The CM current is about 13.3mA, and the SWR for the DM current is 2.34.

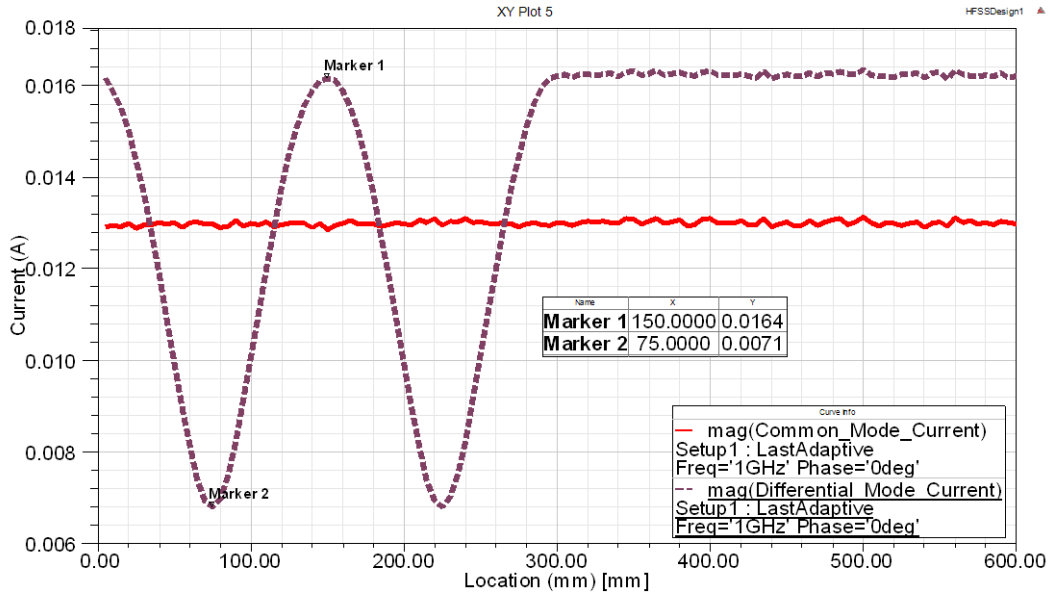


Fig.2. 31. HFSS calculation result.

Table 2.2. Comparison of calculation result with different method.

	Full wave simulation by HFSS	IDT model with conversion impedance	IDT model without conversion impedance
Calculated CM current	13.3 mA	13.8 mA	18.3 mA
SWR	2.34	2.36	N/A

Table 2.2 shows the comparison of the calculated results from the full wave simulation, the IDT model results with the conversion impedance and the IDT model results without accounting for the conversion impedance. There is good agreement (within 4% or 0.3 dB) between the IDT result including the conversion impedance and the full wave simulation.

2.6 Conclusion

This paper has presented a rigorous derivation of the imbalance difference theory, including expressions for the mode conversion impedances, for a three-conductor TL

where one of the conductors is designated as the zero-volt reference or ground conductor. The voltages and currents on the conductors can be related to DM and CM modes of propagation that are independent and orthogonal using Equations (41)-(44). Any changes in the electrical balance, as defined by Equation (17), along the TL result in coupling between the DM and CM modes. A model describing the DM-to-CM coupling was derived in Section 4.1. The change in the CM voltage at an interface is equal to the DM voltage at the interface times the change in the imbalance factor. A model describing the CM-to-DM coupling was derived in Section 4.2. The change in the DM current at an interface is equal to the CM current at the interface times the change in the imbalance factor. The conversion impedances have little impact on the calculated coupling if the converted power is a small percentage of the signal power(i.e. the coupling between the modes is weak). However, the example in Section 5 demonstrates that the conversion impedance can have a significant effect on differential-mode signals when there is a significant discontinuity in the balance, even when the characteristic impedance is maintained.

References

- [1] C. R. Paul, "A comparison of the contributions of common-mode and differential-mode currents in radiated emissions," *IEEE Trans. Electromagn. Compat.*, vol. 31, no. 2, pp. 189–193, May 1989.
- [2] G. I. Zysman and A. K. Johnson, "Coupled Transmission Line Networks in an Inhomogeneous Dielectric Medium," *IEEE Trans. Microw. Theory Tech.*, vol. 17, no. 10, pp. 753–759, Oct. 1969.
- [3] K. D. Marx, "Propagation Modes, Equivalent Circuits, and Characteristic Terminations for Multiconductor Transmission Lines with Inhomogeneous

- Dielectrics,” *IEEE Trans. Microw. Theory Tech.*, vol. 21, no. 7, pp. 450–457, Jul. 1973.
- [4] V. K. Tripathi, “Asymmetric Coupled Transmission Lines in an Inhomogeneous Medium,” *IEEE Trans. Microw. Theory Tech.*, vol. 23, no. 9, pp. 734–739, Sep. 1975.
- [5] G. I. Zysman and A. K. Johnson, “Coupled Transmission Line Networks in an Inhomogeneous Dielectric Medium,” *IEEE Trans. Microw. Theory Tech.*, vol. 17, no. 10, pp. 753–759, Oct. 1969.
- [6] S. B. Cohn, “Shielded Coupled-Strip Transmission Line,” *IEEE Trans. Microw. Theory Tech.*, vol. 3, no. 5, pp. 29–38, Oct. 1955.
- [7] R. A. Speciale, “Fundamental Even- and Odd-Mode Waves for Nonsymmetrical Coupled Lines in Non-Homogeneous Media,” in *S-MTT International Microwave Symposium Digest*, 1974, vol. 74, no. 1, pp. 156–158.
- [8] D. E. D. E. Bockelman, W. R. W. R. Eisenstadt, and S. Member, “Combined differential and common-mode scattering parameters: theory and simulation,” *IEEE Trans. Microw. Theory Tech.*, vol. 43, no. 7, pp. 1530–1539, Jul. 1995.
- [9] F. B. M. Van Horck, A. P. J. Van Deursen, and P. C. T. Van der Laan, “Common-mode currents generated by circuits on a PCB-measurements and transmission-line calculations,” *IEEE Trans. Electromagn. Compat.*, vol. 43, no. 4, pp. 608–617, 2001.
- [10] J. Brown and B. Whitlock, “Common-Mode to Differential-Mode Conversion in Shielded Twisted-Pair Cables (Shield-Current-Induced Noise),” *Audio Eng. Soc. Conv. 114*, 2003.
- [11] a. Vukicevic, M. Rubinstein, F. Rachidi, and J.-L. Bermudez, “On the mechanisms of differential-mode to common-mode conversion in the broadband over power line (BPL) frequency band,” *2006 17th Int. Zurich Symp. Electromagn. Compat.*, pp. 658–661, 2006.
- [12] P. Favre, C. Candolfi, M. Schneider, M. Rubinstein, P. Krahenbuehl, and A. Vukicevic, “Common mode current and radiations mechanisms in PLC networks,” in *2007 IEEE International Symposium on Power Line Communications and Its Applications*, 2007, pp. 348–354.
- [13] T. WATANABE, O. WADA, T. MIYASHITA, and R. KOGA, “Common-Mode-Current Generation Caused by Difference of Unbalance of Transmission Lines on

- a Printed Circuit Board with Narrow Ground Pattern,” *IEICE Trans. Commun.*, vol. E83-B, no. 3, pp. 593–599, Mar. 2000.
- [14] T. Watanabe, O. Wada, Y. Toyota, and R. Koga, “Estimation of common-mode EMI caused by a signal line in the vicinity of ground edge on a PCB,” in *IEEE International Symposium on Electromagnetic Compatibility*, 2002, vol. 1, pp. 113–118.
- [15] T. Watanabe, M. Kishimoto, S. Matsunaga, T. Tanimoto, R. Koga, O. Wada, and A. Namba, “Equivalence of two calculation methods for common-mode excitation on a printed circuit board with narrow ground plane,” in *2003 IEEE Symposium on Electromagnetic Compatibility. Symposium Record (Cat. No.03CH37446)*, 2003, vol. 1, pp. 22–27.
- [16] O. Wada, “Modeling and simulation of unintended electromagnetic emission from digital circuits,” *Electron. Commun. Japan (Part I Commun.)*, vol. 87, no. 8, pp. 38–46, Aug. 2004.
- [17] T. WATANABE, H. FUJIHARA, O. WADA, R. KOGA, and Y. KAMI, “A Prediction Method of Common-Mode Excitation on a Printed Circuit Board Having a Signal Trace near the Ground Edge,” *IEICE Trans. Commun.*, vol. E87-B, no. 8, pp. 2327–2334, Aug. 2004.
- [18] Y. Toyota, A. Sadatoshi, T. Watanabe, K. Iokibe, R. Koga, and O. Wada, “Prediction of electromagnetic emissions from PCBs with interconnections through common-mode antenna model,” in *2007 18th International Zurich Symposium on Electromagnetic Compatibility*, 2007, pp. 107–110.
- [19] Y. Toyota, T. Matsushima, K. Iokibe, R. Koga, and T. Watanabe, “Experimental validation of imbalance difference model to estimate common-mode excitation in PCBs,” in *2008 IEEE International Symposium on Electromagnetic Compatibility*, 2008, pp. 1–6.
- [20] T. MATSUSHIMA, T. WATANABE, Y. TOYOTA, R. KOGA, and O. WADA, “Evaluation of EMI Reduction Effect of Guard Traces Based on Imbalance Difference Model,” *IEICE Trans. Commun.*, vol. E92-B, no. 6, pp. 2193–2200, Jun. 2009.
- [21] T. MATSUSHIMA, T. WATANABE, Y. TOYOTA, R. KOGA, and O. WADA, “Increase of Common-Mode Radiation due to Guard Trace Voltage and Determination of Effective Via-Location,” *IEICE Trans. Commun.*, vol. E92-B, no. 6, pp. 1929–1936, Jun. 2009.

- [22] C. Su and T. H. Hubing, "Imbalance Difference Model for Common-Mode Radiation From Printed Circuit Boards," *IEEE Trans. Electromagn. Compat.*, vol. 53, no. 1, pp. 150–156, Feb. 2011.
- [23] H. Al-Rubaye, K. Pararajasingam, and M. Kane, "Estimating radiated emissions from microstrip transmission lines based on the imbalance model," in *2012 IEEE Electrical Design of Advanced Packaging and Systems Symposium (EDAPS)*, 2012, pp. 93–96.
- [24] H. Kwak and T. H. Hubing, "Investigation of the imbalance difference model and its application to various circuit board and cable geometries," in *2012 IEEE International Symposium on Electromagnetic Compatibility*, 2012, pp. 273–278.
- [25] T. Matsushima, O. Wada, T. Watanabe, Y. Toyota, and L. R. Koga, "Verification of common-mode-current prediction method based on imbalance difference model for single-channel differential signaling system," in *2012 Asia-Pacific Symposium on Electromagnetic Compatibility*, 2012, vol. 2, pp. 409–412.
- [26] T. Matsushima and O. Wada, "A method of common-mode reduction based on imbalance difference model for differential transmission line bend," *Electromagn. Compat. (EMC ...)*, pp. 338–341, 2013.
- [27] Seungyong Baek, Seungyoung Ahn, Jongbae Park, Joungho Kim, Jonghoon Kim, and Jeong-hyeon Cho, "Accurate high frequency lossy model of differential signal line including mode-conversion and common-mode propagation effect," *2004 Int. Symp. Electromagn. Compat. (IEEE Cat. No.04CH37559)*, vol. 2, pp. 562–566, 2004.
- [28] Y. Toyota, K. Iokibe, and L. R. Koga, "Mode conversion caused by discontinuity in transmission line: From viewpoint of imbalance factor and modal characteristic impedance," in *2013 IEEE Electrical Design of Advanced Packaging Systems Symposium (EDAPS)*, 2013, pp. 52–55.
- [29] "atlc2 - Arbitrary Transmission Line Calculator." [Online]. Available: <http://www.hdtvprimer.com/KQ6QV/atlc2.html>. [Accessed: 12-Aug-2014].
- [30] "ANSYS HFSS." [Online]. Available: <http://www.ansys.com/Products/Simulation+Technology/Electronics/Signal+Integrity/ANSYS+HFSS>. [Accessed: 20-Aug-2014].
- [31] C. Paul, *Analysis of multiconductor transmission lines*, 2nd Editio. Hoboken, NJ: Wiley & Sons, Inc, 2008, pp. 160–165.

Appendix: Derivation of imbalance factor in terms of impedances.

The measure of the electrical balance of a TL is called the imbalance factor, “ h ”. “ h ” is also the current division factor. It is defined as, when launching a CM current on a two conductor transmission line (TL), the ratio of current flows on one conductor over the total current flows on both conductors [13]:

$$h = \frac{I_{C1}}{I_{C1} + I_{C2}} \quad (58)$$

In Equation (58), I_{C1} and I_{C2} denote the part of the CM currents flow on each of the two conductor of the TL.

For a lossless two-conductor transmission line with uniform cross section at the vicinity of a reference plane, we can model it as lumped L-C circuit as shown in Fig.2.32, where all the inductances and capacitances are expressed in Henry per unit length and Farad per unit length separately.

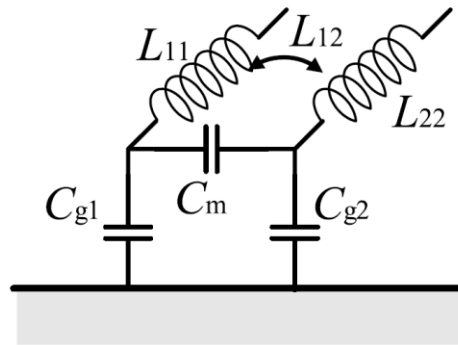


Fig.2.32. Lumped LC model for a cross section of TL.

Watanabe showed that imbalance factor “ h ” can be calculated either by inductances or capacitances in Fig.2.32[17]

$$h = \frac{C_{g1}}{C_{g1} + C_2} \frac{L_{22} - L_{12}}{L_{11} + L_{22} - 2L_{12}} . \quad (59)$$

If we regard the two conductors and the reference plane as a three-conductor TL, then the capacitance matrix C and inductance matrix L that defined in **Error! Reference source not found.**[31] can be expressed with the parameters in Fig.2.32 as:

$$C = \begin{bmatrix} C_{11} & C_{12} & C_{g1} & C_m & -C_m \\ C_{21} & C_{22} & C_m & C_{g2} + C_m & \end{bmatrix} , \quad (60)$$

$$L = \begin{bmatrix} L_{11} & L_{12} \\ L_{12} & L_{22} \end{bmatrix} . \quad (61)$$

Fig.2.33 shows the matching impedances at one terminal of the three-conductor TL. It can also be regarded as a two port network. I_1 and I_2 are the currents that flows into the system at the two ports (two conductors); V_1 and V_2 are the voltage of the two conductors relative to the reference plane.

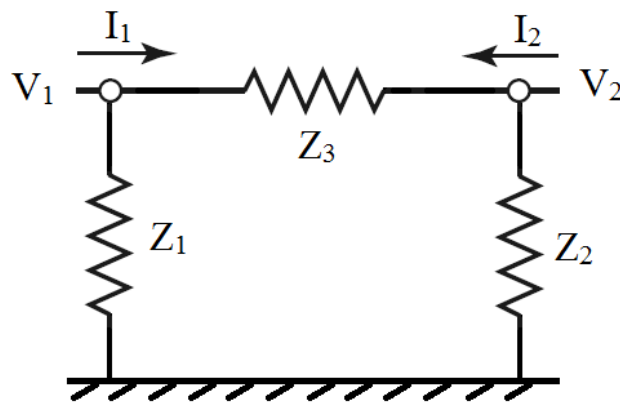


Fig.2.33. Lumped Impedance network of TL.

The following equations hold:

$$I_1 = \frac{V_1}{Z_1} - \frac{V_1 - V_2}{Z_3}, \quad (62)$$

$$I_2 = \frac{V_2}{Z_2} - \frac{V_2 - V_1}{Z_3}. \quad (63)$$

Equation (62) and (63) can be rewrite as,

$$\begin{bmatrix} I_1 \\ I_2 \end{bmatrix} = \begin{bmatrix} \frac{1}{Z_1} & \frac{1}{Z_3} & -\frac{1}{Z_3} \\ \frac{1}{Z_3} & \frac{1}{Z_2} + \frac{1}{Z_3} \end{bmatrix} \cdot \begin{bmatrix} V_1 \\ V_2 \end{bmatrix} \quad (64)$$

The characteristic impedance matrix Z of a three-conductor TL is defined in [31] as the matrix that conforms to equation:

$$\begin{bmatrix} V_1 \\ V_2 \end{bmatrix} = \begin{bmatrix} Z_{11} & Z_{12} \\ Z_{21} & Z_{22} \end{bmatrix} \begin{bmatrix} I_1 \\ I_2 \end{bmatrix}. \quad (65)$$

Compare Equation (64) and(65), we get:

$$Z^{-1} = \begin{bmatrix} \frac{1}{Z_1} & \frac{1}{Z_3} & -\frac{1}{Z_3} \\ \frac{1}{Z_3} & \frac{1}{Z_2} + \frac{1}{Z_3} \end{bmatrix}, \quad (66)$$

$$Z = \frac{1}{\left(\frac{1}{Z_1} + \frac{1}{Z_3}\right) \cdot \left(\frac{1}{Z_2} + \frac{1}{Z_3}\right)} \begin{bmatrix} \frac{1}{Z_2} + \frac{1}{Z_3} & \frac{1}{Z_3} \\ \frac{1}{Z_3} & \frac{1}{Z_1} + \frac{1}{Z_3} \end{bmatrix}. \quad (67)$$

According to [31], for a three-conductor TL, the inductance matrix L , capacitance matrix C and the impedance matrix Z have following relations:

$$Z = v \cdot L , \quad (68)$$

$$Z^{-1} = v \cdot C . \quad (69)$$

Where, “ v ” is the speed of light in the surrounding materials. Equation (68) and (69) can be expanded to:

$$\begin{bmatrix} L_{11} & 12 \\ L_{21} & 22 \end{bmatrix} = \frac{1}{v \left(\frac{1}{Z_1} + \frac{1}{Z_3} \right) \cdot \left(\frac{1}{Z_2} + \frac{1}{Z_3} \right)} \begin{bmatrix} \frac{1}{Z_2} + \frac{1}{Z_3} & \frac{1}{Z_3} \\ \frac{1}{Z_3} & \frac{1}{Z_1} + \frac{1}{Z_3} \end{bmatrix} , \quad (70)$$

$$\begin{bmatrix} C_{11} & 12 \\ C_{21} & 22 \end{bmatrix} = \frac{1}{v} \begin{bmatrix} \frac{1}{Z_1} & \frac{1}{Z_3} & -\frac{1}{Z_3} \\ \frac{1}{Z_3} & \frac{1}{Z_2} + \frac{1}{Z_3} \end{bmatrix} . \quad (71)$$

In Equation (59), if we replace either the C elements or the L elements with the corresponding Z elements in equation (70) or (71), we can get:

$$h = \frac{Z_2}{Z_1 + Z} \quad (72)$$

CHAPTER THREE

MODELING THE LOADING IMPEDANCE ON DIFFERENTIAL MODE SIGNALS DUE TO RADIATED EMISSION

Abstract

Imbalance difference theory describes the conversion mechanism between differential-mode signals and antenna-mode signals on transmission lines. For unintended radiated emission problems, it provides an easy and yet powerful technique to calculate the antenna-mode current that is converted from differential-mode signals. In this paper, we introduce conversion impedance to the existing imbalance difference theory model to account for the loading effect on the differential-mode circuit, so that when the coupling between differential mode and antenna mode are strong, the imbalance difference theory can more accurately estimate the AM current.

3.1 Introduction

Unintended radiated emission is a challenging problem for high speed electronic devices; it has been known for a long time that it is caused by the unintended antenna mode (AM) currents on the cables or other electrically large metal parts. The AM were frequently referred to in the literatures as common mode (CM). We, however, distinguish them in the way that the CM exhibits TEM propagation while the AM does not and it radiates energy away from the structure.

The intended signals on transmission lines are usually differential mode (DM), the fundamental mechanisms by which differential-mode signals are converted to antenna-mode currents on cables attached to printed circuit boards were first studied in [1]–[3], where these mechanisms were described by current-driven models and voltage-driven models. A more precise and easy-to-apply method called Imbalance Difference Theory

(IDT) was introduced later in [4]. IDT pointed out that the unintended antenna-mode current was generated due to a change in the electrical balance of the transmission lines carrying the differential signal currents. The exact antenna-mode current can be accurately calculated based on the transmission line geometries and the strength of the differential-mode signal at the interface.

The IDT has been successfully applied to a number of radiated emission problems since its introduction [5]–[17]. However it wasn't rigorously derived until a recently published paper by the author [xxx], where we demonstrated that if the imbalance factor is defined as the actual current division factor, IDT is strictly correct for radiated emission calculation. We also shown in that paper the conventional method of calculating imbalance factor by analyzing the cross sections of the transmission lines [4] [8] was a very close approximation to the actual current division factor.

For radiated emission problems, the DM and AM signals are usually weakly coupled: only a small portion of the DM energy is converted to AM energy, and the energy converted back to DM is even smaller and can be neglected. For the strong coupling case however, ignoring the energy converted back to DM can affect the accuracy of the calculation. In another recently published paper [xxx], the IDT was applied to a multi-conductor transmission line structure, where the CM signals exhibit TEM propagation and the DM and CM signals are strongly coupled. We introduced the concept of conversion impedance to the IDT model to account for the loading effect to the original DM circuit due to DM-CM conversion.

In this paper we first explore the conversion impedance of IDT model for radiation emission applications. Then we provide an example calculation to show that when the coupling between DM and AM is strong, i.e. when the structure hit resonant frequency, the conversion impedance has big impact over the accuracy of IDT model.

3.2 Imbalance Difference Theory

3.2.1 Imbalance Factor

Consider a two-conductor transmission line with a cross-section that suddenly changes as shown in Fig.3.34. At the interface where the cross-section changes, the voltage between the two conductors is V_{DM} . As described in [x], the change in the electrical balance of the conductors results in an antenna-mode voltage that drives the conductors on one side of the interface relative to the conductors on the other side of the interface as indicated in Fig.3.2. The amplitude of the driving voltage is given by,

$$V_{AM} = \Delta h \cdot (V_{DM}). \quad (73)$$

where Δh is the change in the imbalance factor occurring at the interface and V_{DM} is the differential-mode voltage at the interface. The imbalance factor of each section of the transmission lines is defined as the ratio of the AM currents on each conductor in Fig.3.

35.

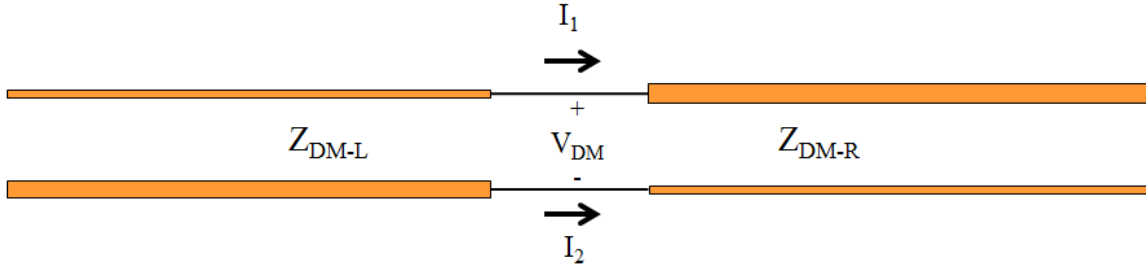


Fig.3.34. Two-conductor transmission lines with changed cross-section.

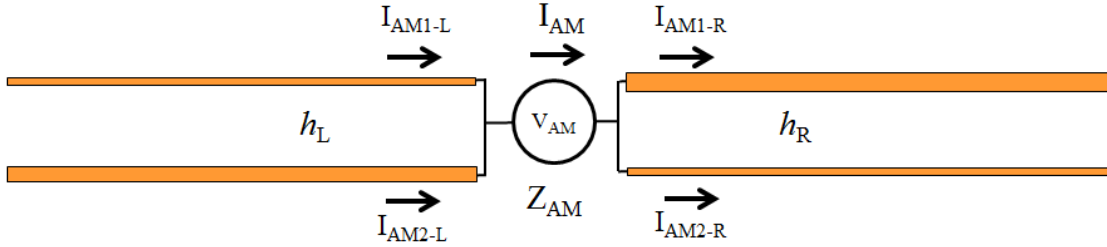


Fig.3. 35. Antenna mode of TLs with divided AM current.

The imbalance factor for left and right section of the TL, h_L and h_R are:

$$h_L = I_{AM1-L} / (I_{AM1-L} + I_{AM2-L}). \quad (74)$$

$$h_R = I_{AM1-R} / (I_{AM1-R} + I_{AM2-R}). \quad (75)$$

The I_{AM-1L} , I_{AM-2L} , I_{AM-1R} , and I_{AM-1R} denote the AM current on each conductor of the TLs in Fig.3. 35.

For realistic radiated emission applications, the current division factor or imbalance factor is hard to obtain precisely, but [xxx] demonstrated that expressing h as a ratio of the per-unit-length inductances or capacitances is a very good approximation.

The equations are:

$$h = \frac{C_{11}}{C_{11} + C_{22}}. \quad (76)$$

$$h = \frac{L_{22} - L_{12}}{L_{11} + L_{22} - 2L_{12}} . \quad (77)$$

Detailed definitions of C_{11} , C_{22} , L_{11} , L_{22} and L_{12} can be found in [8].

3.2.2 Conversion Impedance

The imbalance difference theory describes a method to calculate the conversion between DM and CM/AM signals [4] [8]. It points out that the conversion from one mode to the other is due to the change of electrical balance along the transmission lines and the strength of the conversion is proportional to the change of the imbalance factor.

Based on IDT, for the circuit in Fig.3.34, the generated AM current will be equal to that in Fig. 3. 35 when the AM voltage source is:

$$V_{AM} = V_{DM} \cdot (h_R - h_L) . \quad (78)$$

If we denote the input impedance of the antenna that the AM voltage source sees in Fig.3. 35 as Z_{AM} , then the AM current is:

$$I_{AM} = V_{AM} / Z_{AM} = V_{DM} \cdot (h_R - h_L) / Z_{AM} . \quad (79)$$

According to the IDT, at the interface where imbalance factor changes, there will also be conversion from AM current to DM current as:

$$\Delta I_{DM} = -I_{AM} \cdot (h_R - h_L) = -V_{DM} \cdot (h_R - h_L)^2 / Z_{AM} . \quad (80)$$

The extra DM current, ΔI_{DM} , virtually flows from one conductor to the other at the interface, as shown in Fig.3.36. Its effect over the DM circuit can be represented by an impedance, which we call conversion impedance, Z_{DA} , as shown in Fig.3.37.

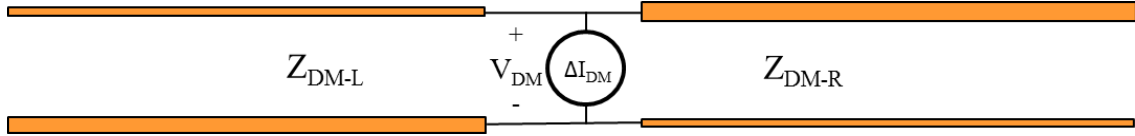


Fig.3.36. DM circuit with the extra virtual DM current.

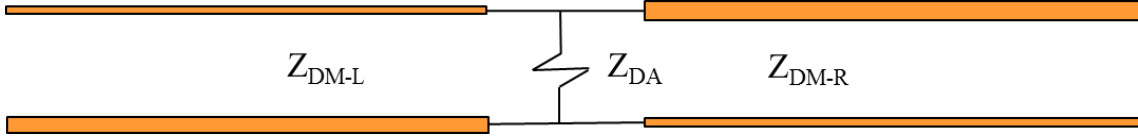


Fig.3.37. DM circuit with the conversion impedance.

The expression for the conversion impedance is:

$$Z_{DA} = \frac{V_{DM}}{|\Delta I_{DM}|} = \frac{Z_{AM}}{(h_R - h_L)^2}. \quad (81)$$

3.3 Experimental Validation

3.3.1 Example Structure and Measurement Setup

As shown in Fig.3.38, we connected a twisted wire pair (TWP) to a coaxial cable and kept the structure standing vertically on a metal ground plane. The structure was fed by a DM voltage through underground coaxial cable. The change of electrical balance at the interface between the coaxial cable and the TWP produces AM current. The AM current was measured at the bottom of the antenna close to the ground surface. The feeding DM voltage was measured by an oscilloscope through a T-connector.

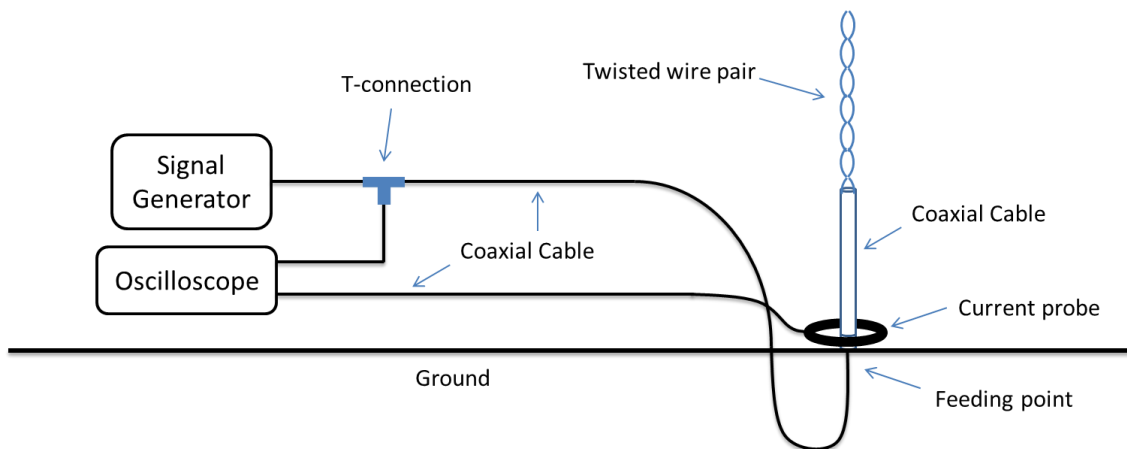


Fig.3.38. Validation structure and measurement set up.

Fig.3.39 is a photo of the test setup. The tested TWP and coaxial cable were placed in a semi-anechoic chamber and the coaxial cables used for feeding and measurement were placed close to the ground plane so that they had very little effect on the antenna. Measurement set-up parameters are listed in Table.3.1.



Fig.3.39. Validation structure and measurement set up.

Table.3.1. Parameters of measurement setup.

TWP wire	AWG 18 (conductor diameter: 1mm, insulator thickness 0.75mm)
----------	--

Coaxial cable	RG-58AU
Standing coaxial cable length	0.5 meter
TWP length	0.5 meter
Length of coaxial cable from the feeding point to the T-connection	1.41 meter
Signal generator	BK precision 4087
Oscilloscope	Tektronix MSO 4104
Current probe	Fisher F-33-1
Measured wave velocity of propagation in the TWP	$2.0 \cdot 10^8 \text{ m/s}$
TWP termination	Open circuit

3.3.2 Calculation Procedure

The structure in Fig.3.38 can be modeled as the circuit shown in Fig.3.40. The goal of the first part of the calculation is to determine the DM voltage at the interface where the TWP and coaxial cable connect so that we can apply IDT to calculate the equivalent AM voltage source that drives the TWP-coaxial-cable antenna.

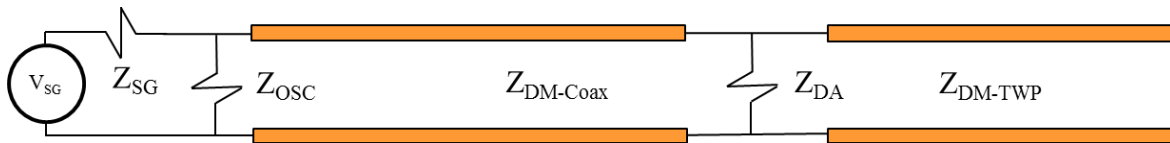


Fig.3.40. Equivalent circuit for measurement set up.

The characteristic impedance of the twisted wire pair, Z_{DM-TWP} can be calculated by:

$$Z_{DM-TWP} = \frac{120}{\sqrt{\epsilon_r}} \cdot \ln\left(\frac{2 \cdot s}{d}\right). \quad (82)$$

where ϵ_r is the relative permittivity of the insulation material; s is the distance between the centers of two wires, d is the diameter of the conductor in the wires.

$Z_{DM-Coax}$, Z_{OSC} , and Z_{SG} are the characteristic impedance of the coaxial cable, the input impedance of the oscilloscope and the output impedance of the signal generator, respectively. They are all 50ohms . The twisted wire pair is a typical balanced transmission line and the imbalance factor, h_{TWP} , is 0.5. The coaxial cable is a typical perfectly unbalanced transmission line and the imbalance factor, h_{Coax} , is 1.

The change of imbalance factor at the interface where TWP connects to the coaxial cable is,

$$\Delta h = h_{Coax} - h_{TWP} = 0.5 . \quad (83)$$

The Z_{DA} in Fig.3.40 is the DM-to-AM conversion impedance. It can be calculated using (81). The input impedance of the antenna was calculated using the antenna modeling software, 4NEC2 [18], where solid wires were used to represent the TWP and the coaxial cable. The equivalent radius used for the coaxial cable was the same as the cable-shield's radius; the one used for the TWP was calculated as [19]:

$$R_{TWP} = \sqrt{s \cdot d / 2} . \quad (84)$$

The input impedance looking into the TWP from the interface is,

$$Z_{in-TWP} = Z_{DM-TWP} \cdot \frac{1}{j \cdot \tan(\beta_{TWP} \cdot l_{TWP})} , \quad (85)$$

where l_{TWP} is the length of the TWP and β_{TWP} is the phase constant of the TWP.

The load impedance that the coaxial cable sees at the interface is,

$$Z_{L-mid} = Z_{DA} \parallel Z_{in-TWP} . \quad (86)$$

The input impedance looking into the coaxial cable is,

$$Z_{in-Coax} = Z_{DM-Coax} \cdot \frac{Z_{L-mid} + j \cdot Z_{DM-Coax} \cdot \tan(\beta_{Coax} \cdot l_{Coax})}{Z_{DM-Coax} + j \cdot Z_{L-mid} \cdot \tan(\beta_{Coax} \cdot l_{Coax})} . \quad (87)$$

where β_{coax} is the phase constant of the coaxial cable and the l_{Coax} is the length of the coaxial cable from the interface where it connects to the TWP to the T-connection.

The DM voltage at the T-connection that feeds the coaxial cable can be calculated as,

$$V_{coax-feed} = V_{SG} \cdot \frac{Z_{in-Coax} \parallel Z_{OSC}}{Z_{in-Coax} \parallel Z_{OSC} + Z_{SG}} . \quad (88)$$

The reflection coefficient at the interface where coaxial cable connects to TWP is,

$$\Gamma_{mid} = \frac{Z_{L-mid} - Z_{DM-Coax}}{Z_{L-mid} + Z_{DM-Coax}} . \quad (89)$$

So the positive propagation voltage at the interface is,

$$V_{mid}^+ = \frac{V_{coax-feed}}{e^{j \cdot \beta_{coax} \cdot l_{coax}} + \Gamma \cdot e^{-j \cdot \beta_{coax} \cdot l_{coax}}} . \quad (90)$$

and the DM voltage at the interface is,

$$V_{DM} = V_{mid}^+ + V_{mid}^+ \cdot \Gamma . \quad (91)$$

Applying IDT yields the equivalent AM voltage source that drives the antenna:

$$V_{AM} = V_{DM} \cdot \Delta h . \quad (91)$$

With the equivalent AM voltage source, we build the structure similar as that in 4nec2 in a MOM simulation software, FEKO [20], to calculate the AM current at the bottom of the antenna.

3.3.3 Comparison between Calculation Results and Measurement Results

We calculated the DM voltage that feeds the coaxial cable at the T-connection in Fig.3.38 and the AM current at the bottom of the antenna. The IDT was applied both with and without conversion impedance Z_{DA} . The comparisons of the calculated results and the measurement results are shown in Fig.3.41 and Fig.3.42.

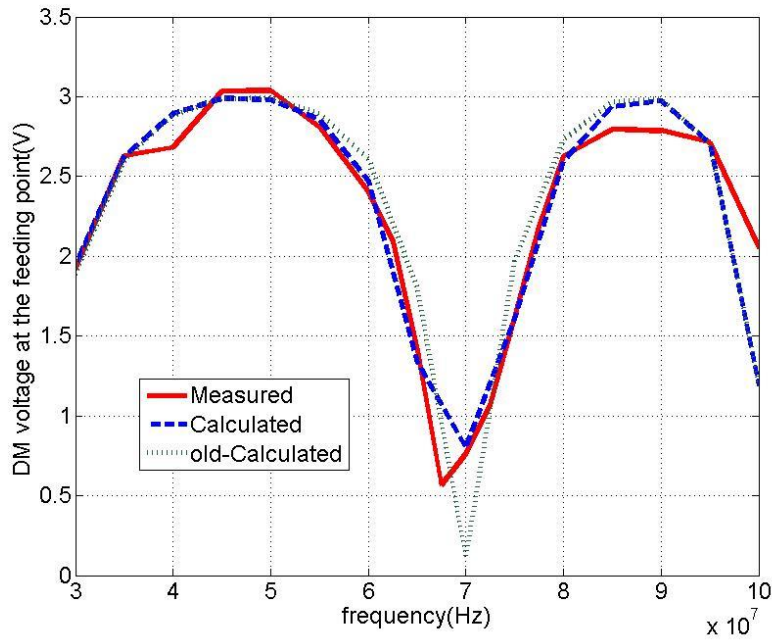


Fig.3.41. Comparison of DM voltage at the T-connection.

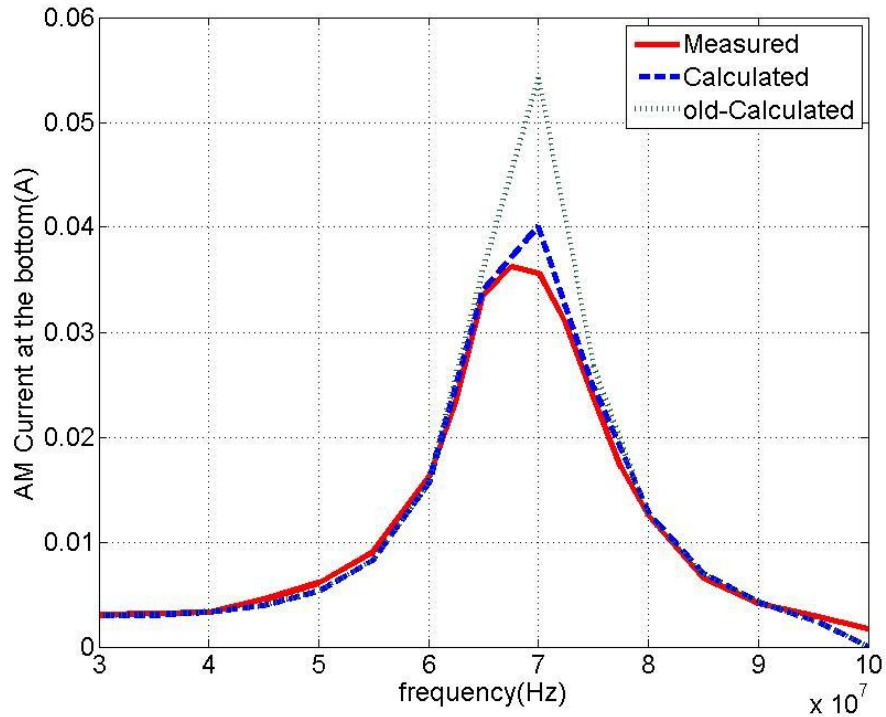


Fig.3.42. Comparison of AM current at the bottom of the antenna.

We can see from Fig.3.41 and Fig.3.42 that the calculated results with conversion impedance, labelled as “Calculated” in the plots, are very close to the measurement result over the frequency from 30MHz to 100MHz. The results without conversion impedance, noted as “old-Calculated” in both plots, are very close to tfig.2.hat with conversion impedance over most of the frequency range except at resonant frequency, around 70MHz, where the old model over-estimated the AM current.

Here is the explanation: According to (81), the conversion impedance is proportional to the input impedance of the antenna, Z_{AM} , in our case, it is 4 times of Z_{AM} . At non-resonant frequencies, Z_{AM} is about couple hundreds ohms, which can be seen on an input-impedance-over-frequency plot on Fig.3.43, so the Z_{DA} is much bigger than the DM impedances. At resonant frequency, however, the input impedance is about 70 ohms

and the Z_{DA} is less than 300 ohms, which is comparable to the DM impedances, as a result neglecting Z_{DA} causes less accurate calculation results.

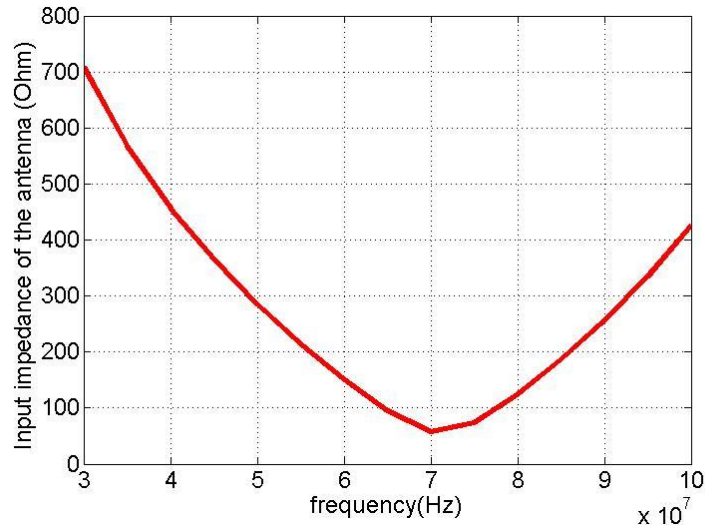


Fig.3.43. Input impedance of the antenna seen by the AM voltage source.

3.4 Conclusion

In this paper we introduce the conversion impedance to the imbalance difference theory for modelling radiated emissions. For most practical radiating structures, at non-resonant frequencies, the conversion impedance is much larger than the DM impedances in the circuit and it has little impact over the accuracy of IDT models. However, we demonstrate with an example structure that the conversion impedance can have big influence over the accuracy of the IDT model if the radiating structure hits resonant frequency and the conversion impedance becomes comparable to the DM impedances.

References

- [1] J. L. Drewniak, T. H. Hubing, and T. P. Van Doren, "Investigation of fundamental mechanisms of common-mode radiation from printed circuit boards with attached

- cables,” in *Proceedings of IEEE Symposium on Electromagnetic Compatibility*, 1994, pp. 110–115.
- [2] J. L. Drewniak, T. P. Van Doren, T. H. Hubing, and J. Shaw, “Diagnosing and modeling common-mode radiation from printed circuit boards with attached cables,” in *Proceedings of International Symposium on Electromagnetic Compatibility*, 1995, vol. 1, pp. 465–470.
- [3] D. M. Hockanson, J. L. Drewniak, T. H. Hubing, T. P. Van Doren, and M. J. Wilhelm, “Investigation of fundamental EMI source mechanisms driving common-mode radiation from printed circuit boards with attached cables,” *IEEE Trans. Electromagn. Compat.*, vol. 38, no. 4, pp. 557–566, 1996.
- [4] T. WATANABE, O. WADA, T. MIYASHITA, and R. KOGA, “Common-Mode-Current Generation Caused by Difference of Unbalance of Transmission Lines on a Printed Circuit Board with Narrow Ground Pattern,” *IEICE Trans. Commun.*, vol. E83-B, no. 3, pp. 593–599, Mar. 2000.
- [5] T. Watanabe, O. Wada, Y. Toyota, and R. Koga, “Estimation of common-mode EMI caused by a signal line in the vicinity of ground edge on a PCB,” in *IEEE International Symposium on Electromagnetic Compatibility*, 2002, vol. 1, pp. 113–118.
- [6] T. Watanabe, M. Kishimoto, S. Matsunaga, T. Tanimoto, R. Koga, O. Wada, and A. Namba, “Equivalence of two calculation methods for common-mode excitation on a printed circuit board with narrow ground plane,” in *2003 IEEE Symposium on Electromagnetic Compatibility. Symposium Record (Cat. No.03CH37446)*, 2003, vol. 1, pp. 22–27.
- [7] O. Wada, “Modeling and simulation of unintended electromagnetic emission from digital circuits,” *Electron. Commun. Japan (Part I Commun.)*, vol. 87, no. 8, pp. 38–46, Aug. 2004.
- [8] T. Watanabe, H. Fujihara, O. Wada, R. Koga, and Y. Kami, “A Prediction Method of Common-Mode Excitation on a Printed Circuit Board Having a Signal Trace near the Ground Edge,” *IEICE Trans. Commun.*, vol. E87-B, no. 8, pp. 2327–2334, Aug. 2004.
- [9] Y. Toyota, A. Sadatoshi, T. Watanabe, K. Iokibe, R. Koga, and O. Wada, “Prediction of electromagnetic emissions from PCBs with interconnections through common-mode antenna model,” in *2007 18th International Zurich Symposium on Electromagnetic Compatibility*, 2007, pp. 107–110.

- [10] Y. Toyota, T. Matsushima, K. Iokibe, R. Koga, and T. Watanabe, "Experimental validation of imbalance difference model to estimate common-mode excitation in PCBs," in *2008 IEEE International Symposium on Electromagnetic Compatibility*, 2008, pp. 1–6.
- [11] T. Matsushima, T. Watanabe, Y. Toyota, R. Koga, and O. Wada, "Increase of Common-Mode Radiation due to Guard Trace Voltage and Determination of Effective Via-Location," *IEICE Trans. Commun.*, vol. E92-B, no. 6, pp. 1929–1936, Jun. 2009.
- [12] T. Matsushima, T. Watanabe, Y. Toyota, R. Koga, and O. Wada, "Evaluation of EMI Reduction Effect of Guard Traces Based on Imbalance Difference Model," *IEICE Trans. Commun.*, vol. E92-B, no. 6, pp. 2193–2200, Jun. 2009.
- [13] C. Su and T. H. Hubing, "Imbalance Difference Model for Common-Mode Radiation From Printed Circuit Boards," *IEEE Trans. Electromagn. Compat.*, vol. 53, no. 1, pp. 150–156, Feb. 2011.
- [14] H. Kwak and T. H. Hubing, "Investigation of the imbalance difference model and its application to various circuit board and cable geometries," in *2012 IEEE International Symposium on Electromagnetic Compatibility*, 2012, pp. 273–278.
- [15] T. Matsushima, O. Wada, T. Watanabe, Y. Toyota, and L. R. Koga, "Verification of common-mode-current prediction method based on imbalance difference model for single-channel differential signaling system," in *2012 Asia-Pacific Symposium on Electromagnetic Compatibility*, 2012, vol. 2, pp. 409–412.
- [16] A. Sugiura and Y. Kami, "Generation and Propagation of Common-Mode Currents in a Balanced Two-Conductor Line," *IEEE Trans. Electromagn. Compat.*, vol. 54, no. 2, pp. 466–473, Apr. 2012.
- [17] H. Al-Rubaye, K. Pararajasingam, and M. Kane, "Estimating radiated emissions from microstrip transmission lines based on the imbalance model," in *2012 IEEE Electrical Design of Advanced Packaging and Systems Symposium (EDAPS)*, 2012, pp. 93–96.
- [18] "4nec2." [Online]. Available: <http://www.qsl.net/4nec2/>.
- [19] C. A. Balanis, "Antenna Theory, Analysis and Design," 2nd Edition, John Willey & Sons, Inc. 1997, p. 456.
- [20] *FEKO User's Manual*, Suite 6.2. 2013.